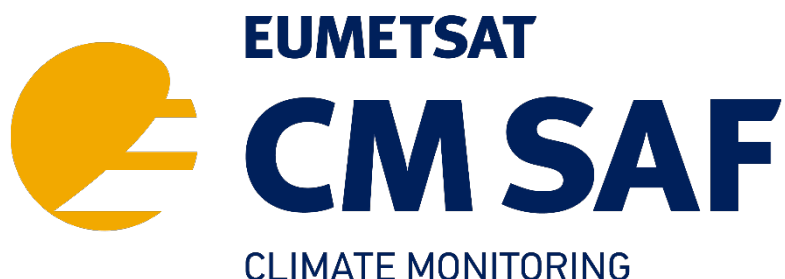


EUMETSAT Satellite Application Facility on Climate Monitoring



Product User Manual SEVIRI cloud products CLAAS Edition 3

DOI: [10.5676/EUM_SAF_CM/CLAAS/V003](https://doi.org/10.5676/EUM_SAF_CM/CLAAS/V003)

	TCDR	ICDR
Fractional Cloud Cover (CFC)	CM-21014	CM-5011
Joint Cloud property Histogram (JCH)	CM-21023	CM-5021
Cloud Top level (CTO)	CM-21033	CM-5031
Cloud Phase (CPH)	CM-21043	CM-5041
Liquid Water Path (LWP)	CM-21053	CM-5051
Ice Water Path (IWP)	CM-21063	CM-5061

Reference Number:
Issue/Revision Index:
Date:

SAF/CM/KNMI/PUM/SEV/CLD
3.1
08.08.2022

Document Signature Table

	Name	Function	Signature	Date
Authors	Jan Fokke Meirink	CM SAF scientist (KNMI)		08/08/2022
	Martin Stengel	CM SAF scientist (DWD)		
	Nikos Benas	CM SAF scientist (KNMI)		
	Irina Solodovnik	CM SAF scientist (DWD)		
	Nina Håkansson	CM SAF scientist (SMHI)		
	Karl-Göran Karlsson	CM SAF scientist (SMHI)		
Editor	Marc Schröder	Science Coordinator		08/08/2022
Approval	CM SAF Steering Group			
Release	Rainer Hollmann	Project Manager		


Distribution List

Internal Distribution	
Name	No. Copies
DWD Archive	1
CM SAF Team	1

External Distribution		
Company	Name	No. Copies
PUBLIC		1

Document Change Record

Issue/ Revision	Date	DCN No.	Changed Pages/Paragraphs
3.0	20/05/2022	SAF/CM/KNMI/PUM/SEV/CLD /3.0	First official version submitted for DRR 3.7 and ORR3.4

	Product User Manual SEVIRI cloud products CLAAS Edition 3	Doc. No: SAF/CM/KNMI/PUM/SEV/CLD Issue: 3.1 Date: 08.08.2022
---	--	--

3.1	08/08/2022	SAF/CM/KNMI/PUM/SEV/CLD /3.1	Version after DR/ORR, with RID responses implemented
-----	------------	------------------------------	--

Applicable Documents

Reference	Title	Code / Date
AD 1	EUMETSAT CM SAF CDOP 3 Product Requirements Document (PRD)	SAF/CM/DWD/PRD/4.0
AD 2	Requirements Review SEVIRI Edition 3 data records (CLAAS Edition 3)	SAF/CM/CDOP3/KNMI/RR37

Reference Documents

Reference	Title	Code
RD 1	Product User Manual SEVIRI Cloud Products Edition 3 (CLAAS-3)	SAF/CM/DWD/PUM/SEV/CLD/3.0
RD 2	Algorithm Theoretical Basis Document SEVIRI cloud products processing chain	SAF/CM/DWD/ATBD/SEV/CLD/3.2
RD 3	Algorithm Theoretical Basis Document (An Appendix to the NWC/PPS) Cloud Probability and Cloud Top Temperature/Height from SEVIRI	SAF/CM/SMHI/ATBD/SEV/PPSSEV/3.2
RD 4	Algorithm Theoretical Basis Document SEVIRI cloud physical products	SAF/CM/KNMI/ATBD/SEV/PPP/3.2
RD 5	Data Set Generation Capability Description Document, CLAAS Edition 3	SAF/CM/DWD/DGCDD/CLAAS/3.2
RD 6	Operation Procedures Document (OPD)	SAF/CM/DWD/OPD/CLAAS, v1.0

Table of Contents

1	Executive Summary	8
2	The EUMETSAT SAF on Climate Monitoring (CM SAF).....	10
3	Compilation of the CLAAS-3 cloud dataset.....	12
3.1	Product definitions	14
3.2	Main changes compared to CLAAS-2.1	16
4	Product description.....	17
4.1	Fractional cloud cover – CFC.....	17
4.2	Cloud Top level – CTO	20
4.3	Cloud Phase – CPH.....	24
4.4	Liquid Water Path – LWP.....	26
4.5	Ice Water Path – IWP	30
4.6	Joint Cloud property Histogram – JCH.....	32
5	Summary table of validation results regarding product accuracy	35
6	Summary and outlook	37
7	Data format description	38
7.1	Data format description of non-averaged products.....	38
7.1.1	General variables.....	38
7.1.2	Common attributes	39
7.1.3	Product specific data fields	39
7.1.3.1	Cloud mask (CMA).....	40
7.1.3.2	Cloud top (CTX).....	40
7.1.3.3	Cloud physical properties (CPP)	40
7.1.4	Global attributes	42
7.1.5	Auxiliary data	44
7.2	Monthly and daily mean data file contents	46
7.2.1	General variables.....	46
7.2.2	Common attributes	47

7.2.3	Product specific data fields	47
7.2.3.1	Fractional cloud coverage (CFC)	47
7.2.3.2	Cloud phase (CPH).....	49
7.2.3.3	Cloud top level (CTO)	50
7.2.3.4	Liquid water path (LWP).....	54
7.2.3.5	Ice water path (IWP)	59
7.2.3.6	Joint Cloud property Histograms (JCH).....	64
7.2.3.7	One-dimensional histograms.....	64
7.2.3.8	Mean diurnal cycle	66
7.2.4	Global attributes	67
8	Data ordering via the Web User Interface (WUI)	70
8.1	Product ordering process.....	70
8.2	Contact User Help Desk staff.....	70
8.3	Feedback/User Problem Report.....	70
8.4	Service Messages / log of changes.....	70
9	Copyright and Disclaimer	71
10	References.....	72
11	Acronyms	76

List of Tables

Table 3-1: CLAAS-3 product suite.	14
Table 3-2: L3 product features including day and night separation, liquid water and ice separation, and histogram representation. Please note that the LWP and IWP histograms are combined in one product (CWPmh), see section 7.2.3.7.	15
Table 5-1: Summary of CLAAS-3 validation results compared to requirements for each cloud product. Required and achieved accuracies are formulated in terms of bias, precisions in terms of bc-rmsd (except for CFC and CPH L2, for which the metric is the Hanssen-Kuipers Skill Score, KSS), and stabilities in terms of decadal trend in bias. All numbers, except KSS, are in the units indicated for the respective cloud products. Validation results are color-coded as follows: worse than threshold, fulfils threshold, fulfils target, and fulfils optimal requirement. CALIOP results are reported for different values of (I)COT, the cloud optical thickness integrated from the top of the cloud. Evaluations against MODIS are indicated in grey since they are viewed as consistency checks rather than true validation. CPH, LWP and IWP validation scores are for the 3.9- μ m-based products.	35
Table 7-1: General variables in each L2 product.	38
Table 7-2: Common attributes of each variable in L2 data.	39
Table 7-3: General attributes of a non-averaged NetCDF file.	42
Table 7-4: Contents of the file with auxiliary data, named <i>claas3_level2_aux_data.nc</i>	44
Table 7-5: General variables in each L3 product.	46
Table 7-6: Attributes assigned to each variable in L3 data.	47
Table 7-7: Overview of global attributes of NetCDF files of CLAAS-3 products and possible corresponding values.	67

List of Figures

Figure 3-1: Illustration of the CLAAS-3 TCDR and ICDR temporal coverage.....	12
Figure 3-2: Overview of the SEVIRI measurement record used as basis for the cloud generation of the CLAAS-3 TCDR. Short-term data gaps are shown enlarged by a factor of 5 for better visibility.....	13
Figure 3-3: SEVIRI spatial coverage and on-ground resolution expressed as the edge length of a square having the same area as the SEVIRI grid cell.....	13
Figure 4-1: CLAAS-3 L2 instantaneous binary cloud mask (top left) and cloud probability (top right) for 1 June 2010 12:00 UTC, and L3 monthly mean cloud fractional cover (bottom left) and the corresponding mean uncertainty for June 2010 (bottom right). Note that the majority of pixels have cloud probabilities close to 0 or 100%, so the top left and right panels look similar.	17
Figure 4-2: Time series of the 45° W-E and S-N area-averaged cloud fractional cover from CLAAS-3 and Aqua MODIS, their biases and the corresponding bc-rmsd. Blue dotted lines in the bias plots show the change in bias (% per decade) based on linear regression.	19
Figure 4-3: CLAAS-3 L2 instantaneous cloud top pressure for 1 June 2010 12:00 UTC (top left) and L3 monthly mean cloud top pressure for June 2010 (bottom left). Corresponding uncertainties are shown on the right.....	20
Figure 4-4: Time series of cloud top height (top) and bias (bottom) from CLAAS-3 and CALIPSO-GEWEX top layer and passive flavor; passive flavor is denoted by dashed line.	22
Figure 4-5: CLAAS-3 L2 instantaneous cloud thermodynamic phase (top left) and extended cloud phase (top right) on 1 June 2010 at 12:00 UTC, and L3 monthly mean cloud thermodynamic phase (bottom left) and its mean standard deviation (bottom right) for June 2010.....	24
Figure 4-6: CLAAS-3 and MODIS fraction of liquid clouds and their difference averaged from 02/2004 until 12/2020.	25
Figure 4-7: CLAAS-3 L2 instantaneous cloud liquid water path on 1 June 2010 at 12:00 UTC (top left) and L3 monthly mean cloud liquid water path for June 2010 (bottom left). Corresponding uncertainties are shown on the right.	26
Figure 4-8: CLAAS-3 and MODIS all-sky liquid water path retrieved based on the 3.9 μm channel and their difference averaged from 02/2004 until 12/2020.....	29
Figure 4-9: CLAAS-3 L2 instantaneous cloud ice water path on 1 June 2010 at 12:00 UTC (top left) and L3 monthly mean cloud ice water path for June 2010 (bottom left). Corresponding uncertainties are shown on the right.	30
Figure 4-10: CLAAS-3 and MODIS all-sky ice water path path retrieved based on the 3.9 μm channel and its difference averaged from 02/2004 until 12/2020.	31
Figure 4-11: JCH, a 2D histogram of cloud top pressure and cloud optical thickness, here aggregated over the 45° S-N, W-E area for 07/2010.	32
Figure 4-12: Map showing the number of the cluster (see Figure 4-13) each grid cell is assigned to.	33

Figure 4-13: Centroid JCH for each of the six clusters, after being scaled by its total number to represent relative frequency of each COT-CTP bin. Also given are the portions of all grid cells belonging to each cluster. 34

1 Executive Summary


This CM SAF Product User Manual provides information on the CLAAS-3 dataset (CLAAS-3: Cloud property dAtAset using SEVIRI, edition 3) derived from Spinning Enhanced Visible and InfraRed Imager (SEVIRI) observations onboard the EUMETSAT METEOSAT Second Generation (MSG) satellites. CLAAS-3 follows the earlier editions CLAAS-1 (Stengel et al. 2014) and CLAAS-2 (Benas et al., 2017). CLAAS-3 consists of a Thematic Climate Data Record (TCDR), spanning the period from 2004 to 2020, and an Interim Climate Data Record (ICDR), starting in 2021 and extended operationally with low latency to the present. The ICDR is produced with the same algorithms as the TCDR but with a few differences in input data (see [RD 2, Section 4.7] for details).

The CLAAS-3 data set contains multiple cloud parameters derived from SEVIRI. The CM SAF release of CLAAS-3 contains the following cloud variables:

	TCDR	ICDR
Fractional Cloud Cover (CFC)	CM-21014	CM-5011
Joint Cloud property Histogram (JCH)	CM-21023	CM-5021
Cloud Top level (CTO)	CM-21033	CM-5031
Cloud Phase (CPH)	CM-21043	CM-5041
Liquid Water Path (LWP)	CM-21053	CM-5051
Ice Water Path (IWP)	CM-21063	CM-5061

Some attractive features of the CLAAS-3 dataset are:

- All atmospheric quantities describing a cloudy atmosphere are highly variable on both, spatial as well as temporal scales. The temporal and spatial resolution of SEVIRI allows a sufficient sampling of every pixel of the SEVIRI disk and can therefore provide accurate estimates of daily and monthly averages of the highly fluctuating quantities. Also, the diurnal cycle of the observed quantities can be described properly which provides further insight into the processes of cloud formation and atmospheric motion. It can also be seen as complementary information to the long-term global cloud property datasets, e.g. CLARA, Cloud_cci, PATMOS-X, MODIS, and ISCCP, with its capability of resolving diurnal cycles, thus providing corresponding uncertainty estimates or even correction in this respect for datasets being exclusively based on polar orbiters.
- The SEVIRI field of view covers a fairly large domain of the globe. For the regions covered (e.g. Europe, Africa, Atlantic Ocean) this allows monitoring climate variability of the considered cloud properties, which becomes more and more mature with SEVIRI's growing measurement record (17 years in this data record).
- The data record is characterized by a very fine spatial resolution of approximately 3 (near the sub-satellite point) to 5 km (e.g. over Europe). This fine resolution is kept in


	Product User Manual SEVIRI cloud products CLAAS Edition 3	Doc. No: SAF/CM/KNMI/PUM/SEV/CLD Issue: 3.1 Date: 08.08.2022
---	--	--

the Level-2 (L2) products (on original SEVIRI projection and resolution), but also in the Level-3 (L3) products (mapped onto a latitude-longitude grid with 0.05° spatial resolution). With this, also small-scale weather and climate features can be resolved and investigated.

CLAAS-3 features many improvements and advantages compared to its second edition, some of the most important ones being:

- The length of the record is 17 years instead of 12 years. Given the good stability of the SEVIRI instrument and the CLAAS-3 record, this is approaching a typical length required for trend analyses.
- CLAAS-3 features various algorithm improvements for all cloud parameters. In particular, the CFC and CTO algorithms have been completely revised.
- More cloud parameters are provided as additional layers, which were not provided for CLAAS-2. An example is cloud droplet number concentration for liquid clouds.

This manual briefly describes the historical development of CM SAF, the CLAAS-3 data record and the versioning for CLAAS-3 products. A technical description of the data records including information on the file format as well as on the data access is provided. Furthermore, details on the implementation of the retrieval processing chain, and individual algorithm descriptions are available in the algorithm theoretical basis documents [RD 2] - [RD 5]. Basic accuracy requirements are defined in the product requirements document [AD 1]. A detailed validation of the SEVIRI based parameters is available in the validation report [RD 1].

	Product User Manual SEVIRI cloud products CLAAS Edition 3	Doc. No: SAF/CM/KNMI/PUM/SEV/CLD Issue: 3.1 Date: 08.08.2022
---	--	--

2 The EUMETSAT SAF on Climate Monitoring (CM SAF)

The importance of satellite-based climate monitoring was recognized in 2000 by EUMETSAT Member States when they amended the EUMETSAT Convention to affirm that the EUMETSAT mandate is also to “contribute to the operational monitoring of the climate and the detection of global climatic changes”. Following this, EUMETSAT established within its Satellite Application Facility (SAF) network a dedicated centre, the SAF on Climate Monitoring (CM SAF, <http://www.cmsaf.eu>).


The consortium of CM SAF currently comprises the Deutscher Wetterdienst (DWD) as host institute, and the partners from the Royal Meteorological Institute of Belgium (RMIB), the Finnish Meteorological Institute (FMI), the Royal Meteorological Institute of the Netherlands (KNMI), the Swedish Meteorological and Hydrological Institute (SMHI), the Meteorological Service of Switzerland (MeteoSwiss), the Meteorological Service of the United Kingdom (UK MetOffice) and the Centre National de la recherche scientifique (CNRS) of France. Since the beginning in 1999, the EUMETSAT Satellite Application Facility on Climate Monitoring (CM SAF) has developed and will continue to develop capabilities for a sustained generation and provision of Climate Data Records (CDR’s) derived from operational meteorological satellites.

In particular, the generation of long-term data records is pursued. The ultimate aim is to make the resulting data records suitable for the analysis of climate variability and potentially the detection of climate trends. CM SAF works in close collaboration with the EUMETSAT Central Facility and liaises with other satellite operators to advance the availability, quality and usability of Fundamental Climate Data Records (FCDRs) as defined by the Global Climate Observing System (GCOS). As a major task, the CM SAF utilizes FCDRs to produce records of Essential Climate Variables (ECVs) as defined by GCOS. Thematically, the focus of CM SAF is on ECVs associated with the global energy and water cycle.

Another essential task of CM SAF is to produce data records that can serve applications related to the new Global Framework of Climate Services initiated by the WMO World Climate Conference-3 in 2009. CM SAF is supporting climate services at national meteorological and hydrological services (NMHSs) with long-term data records but also with data records produced close to real time that can be used to prepare monthly/annual updates of the state of the climate. Both types of products together allow for a consistent description of mean values, anomalies, variability, and potential trends for the selected ECVs. CM SAF ECV data records also serve the improvement of climate models both at global and regional scale.

As an essential partner in the related international frameworks, the CM SAF assumes the role as main implementer of EUMETSAT’s commitments in support to global climate monitoring. This is achieved through:

- Application of highest standards and guidelines as lined out by GCOS for the satellite data processing,
- Processing of satellite data within an international collaboration benefiting from developments at international level and pollinating the partnership with own ideas and standards,

	Product User Manual SEVIRI cloud products CLAAS Edition 3	Doc. No: SAF/CM/KNMI/PUM/SEV/CLD Issue: 3.1 Date: 08.08.2022
---	--	--

- Intensive validation and improvement of the CM SAF climate data records,
- Taking a major role in data record assessments performed by research organisations such as WCRP (World Climate Research Programme),
- Maintaining and providing an operational and sustained infrastructure that can serve the community within the transition of mature CDR products from the research community into operational environments.

A catalogue of all available CM SAF products is accessible via the CM SAF webpage, www.cmsaf.eu. Here, detailed information about product ordering, add-on tools, sample programs and documentation is provided.

3 Compilation of the CLAAS-3 cloud dataset

The third edition of the CLOUD property dAtAset using SEVIRI (CLAAS-3) is a data record of cloud products derived from measurements taken by the Spinning Enhanced Visible and InfraRed Imager (SEVIRI) onboard the EUMETSAT Meteosat Second Generation (MSG) satellites. CLAAS-3 consists of a Thematic Climate Data Record (TCDR), spanning the period from 2004 to 2020, and an Interim Climate Data Record (ICDR), starting in 2021 and extended operationally with low latency in the present (see Figure 3-1). The ICDR is produced with the same algorithms as the TCDR but with a few differences in input data.

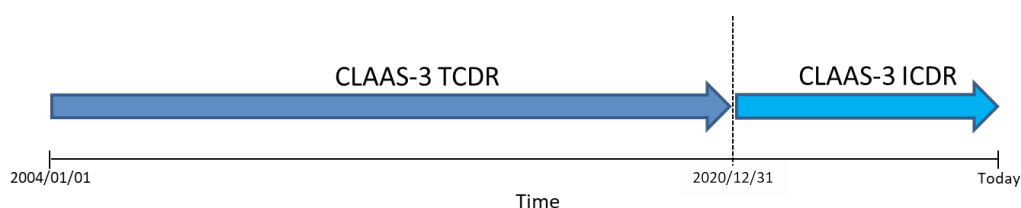


Figure 3-1: Illustration of the CLAAS-3 TCDR and ICDR temporal coverage.

The basis of CLAAS-3 is formed by SEVIRI measurements. SEVIRI is a passive visible and infrared imager mounted on the Meteosat Second Generation (MSG) satellites 1 to 4, also referred to as Meteosat-8 to -11. These are geostationary satellites which, by their rotation, support a SEVIRI imaging repeat cycle of 15 minutes. SEVIRI itself is an optical imaging radiometer with 12 spectral channels ranging from the visible (approximately 0.6 μm) to the infrared at about 13.4 μm .

The CLAAS-3 TCDR covers the time-span 2004-2020, and is based on measurements of MSG-1, MSG-2, MSG-3 and MSG-4 (see Figure 3-2). The respective MSGs in operational mode are most of the time centred near 0°/0° latitude/longitude, where a full earth disk image includes Europe, Africa, the Middle East and the Atlantic Ocean (Figure 3-3). The horizontal resolution of a SEVIRI image is 3 x 3 km² at nadir (Figure 3-3). Gaps of more than 24 hours in the prime satellite were filled by a back-up satellite. For the ICDR, starting in 2021, the input remains the prime operational MSG satellite near 0°/0° latitude/longitude.

For the derivation of cloud products we used the Level 1.5 (L1.5) SEVIRI data provided by EUMETSAT. The L1.5 data record comprises images that have already undergone certain modifications by EUMETSAT: they have been corrected for all unwanted radiometric and geometric effects, geolocated using a standardised projection, and calibrated and radiance-linearized. Because of the introduction of a new radiance definition by EUMETSAT on 5 May 2008, we use reprocessed L1.5 data prior this date with the base algorithm version 0201 and the near real time version 0100 afterwards to ensure homogeneity of the time series.

The L1.5 radiance data record was processed with two software packages: the PPSSEV v2018-patchCMSAF-May2021 software package by the NWC SAF (SAF in support of Nowcasting and Very Short Range Forecasting) used to derive probabilistic cloud mask / cloud fraction and cloud top properties [RD 4], and the CPP (Cloud Physical Properties) algorithm [RD 3], which retrieves cloud thermodynamic phase, cloud optical thickness, cloud particle effective radius, and liquid/ice water path. The CLAAS-3 data record was produced using the infrastructure of the EUMETSAT Weather Cloud (EWC). More details on the TCDR and ICDR processing chains can be found in [RD 5] and [RD 6], respectively.

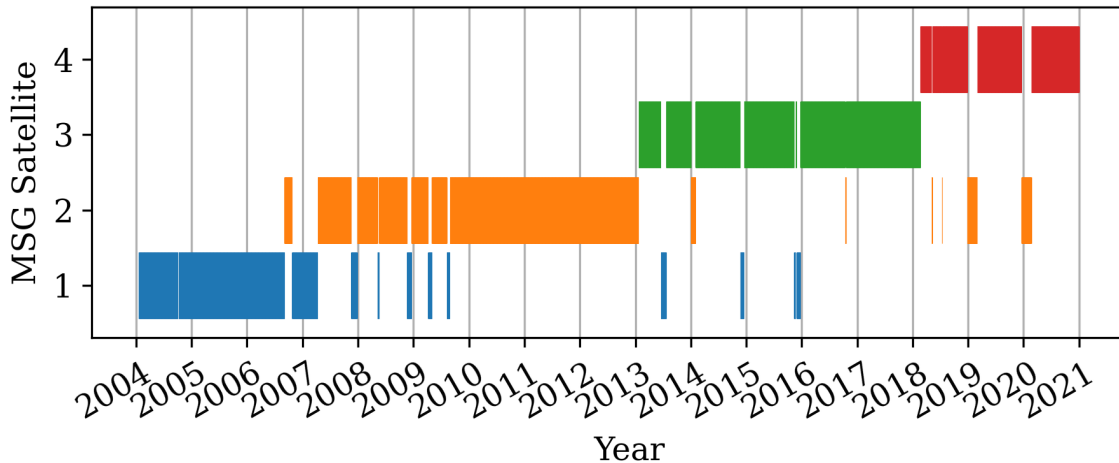


Figure 3-2: Overview of the SEVIRI measurement record used as basis for the cloud generation of the CLAAS-3 TCDR. Short-term data gaps are shown enlarged by a factor of 5 for better visibility.

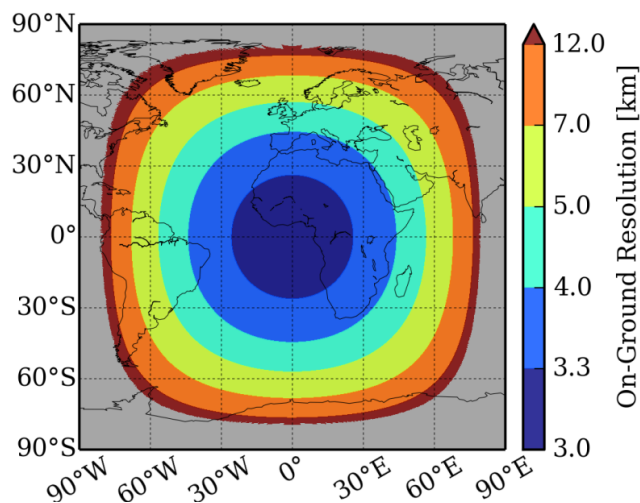


Figure 3-3: SEVIRI spatial coverage and on-ground resolution expressed as the edge length of a square having the same area as the SEVIRI grid cell.

The time series of SEVIRI reflectances was carefully calibrated against the Moderate Resolution Imaging Spectroradiometer (MODIS), which improved especially the retrieval of microphysical parameters. The calibration method is outlined in Meirink et al. (2013). With the calibration also homogenisation was performed because the same MODIS instrument was used for all MSG satellites. The IR radiances of SEVIRI were used as provided by EUMETSAT, relying on the on-board black-body calibration. More details about the SEVIRI L1.5 data are provided in [RD 2].

As shown in Figure 3-2, the prime satellite is occasionally inactive and measurements are then provided by the back-up satellite. Data from these periods (see [RD 2] for exact times) should be considered with some caution because the back-up satellite has a different position and consequently a different viewing geometry, and its shortwave calibration coefficients, being based on an extrapolation of the calibration during its functioning as prime satellite, have a

larger uncertainty. A second warning must be made regarding periods with missing time slots, which will also be characterized by larger uncertainties. Information on missing data can be retrieved from the ‘nobs’ attributes in the product files, indicating the number of pixels and number of days used for aggregation to produce the daily and monthly mean files, respectively. Overall the number of missing time slots is low.

For a more detailed instrument specification and description of the calibration the reader is referred to the Algorithm Theoretical Baseline Document of the SEVIRI cloud products processing chain [RD 2].

3.1 Product definitions

The CLAAS-3 cloud data set from SEVIRI provides six main cloud products. All cloud products, including sublayers, are introduced in Table 3-1 with associated acronyms and units.

All parameters can be accessed on L2 basis, which means in original SEVIRI pixel size (3 x 3 km² at sub-satellite point) and at 15-minute resolution. The products CFC, CPH, CTO, LWP, IWP are also available as daily and monthly composites on a regular latitude/longitude grid with a spatial resolution of 0.05 × 0.05 degrees². Additionally, monthly mean diurnal cycles are provided with a temporal resolution of one hour. Please note that the Joint Cloud property Histogram and the monthly mean diurnal cycle fields are only available on a 0.25 × 0.25 degrees² grid. Also, JCH is available on monthly basis only. All product features are listed in Table 3-2.

Table 3-1: CLAAS-3 product suite.

Product identifier	Acronym	Product title	Unit	
			L2	L3
CM-21014 CM-5011	CFC	Fractional Cloud Cover (or Cloud Amount) (Probabilistic) cloud mask in L2	dimensionless	%
CM-21033 CM-5031	CTO	Cloud Top information: - Cloud Top Pressure - Cloud Top Height - Cloud Top Temperature	hPa m K	hPa m K
CM-21043 CM-5041	CPH	Cloud thermodynamic Phase Liquid or ice cloud in L2 Liquid cloud fraction in L3	dimensionless	%
CM-21053 CM-5051	LWP	Cloud Liquid Water Path	kg/m ²	kg/m ²
	COT	Liquid Cloud Optical Thickness	dimensionless	dimensionless
	CRE	Liquid Cloud droplet Effective Radius	m	m


Product identifier	Acronym	Product title	Unit	
			L2	L3
	CDNC	Cloud Droplet Number Concentration of liquid clouds	m ⁻³	m ⁻³
	CGT	Geometrical Thickness of liquid clouds	m	m
CM-21063 CM-6061	IWP	Cloud Ice Water Path	kg/m ²	kg/m ²
	COT	Ice Cloud Optical Thickness	dimensionless	dimensionless
	CRE	Ice cloud particle Effective Radius	m	m
CM-21023 CM-5021	JCH	Joint Cloud property Histogram, based on CPH, CTP, and COT	dimensionless	dimensionless

Table 3-2: L3 product features including day and night separation, liquid water and ice separation, and histogram representation. Please note that the LWP and IWP histograms are combined in one product (CWPmh), see section 7.2.3.7.

	Daily mean	Monthly mean	Monthly mean diurnal cycle	Monthly histograms
CFC	✓ day/night high/mid/low	✓ day/night high/mid/low	✓	
CTO	✓ day/night liquid/ice	✓ day/night liquid/ice	✓	✓
CPH	✓ day/day+night	✓ day/day+night	✓	
LWP (+ τ , r_e , CDNC, CGT)	✓	✓	✓	✓
IWP (+ τ , r_e)	✓	✓	✓	✓
JCH				✓ liquid/ice

Acknowledging the different observation capabilities during night and during day and also taking into account existing diurnal variations in cloudiness, a further separation of results into daytime and night-time portions was done for CFC, CTO and CPH. Here, all observations made under twilight conditions (solar zenith angles between 75-95 degrees) have been excluded in order to avoid being affected by specific cloud detection problems occurring in the twilight zone. For a full overview of the creation of L3 from L2 products and the filtering applied in this process, we refer to [RD 2].

The temporal coverage of the TCDR ranges from 19.01.2004 to 31.12.2020. To reduce gaps in the data record all products from January 2004 to December 2020 are provided. If a product could not be generated (missing input data, processing failure etc.), an „empty” product containing only fill values was generated. The overall status of each record in a file is stored in the *record_status* variable. In general, *record_status* = 1 denotes an empty product.

	Product User Manual SEVIRI cloud products CLAAS Edition 3	Doc. No: SAF/CM/KNMI/PUM/SEV/CLD Issue: 3.1 Date: 08.08.2022
---	--	--

For each cloud parameter, also various metadata and information about selected statistical parameter distributions in each grid point is available in addition to the main product content described above. Details on how to access this information is given in Section 7.

A complete description of the retrieval methods for each individual product is given in the Algorithm Theoretical Basis Documents [RD 3 and RD 4]. The general methods for SEVIRI calibration and calculation of L3 products are described in [RD 2].

3.2 Main changes compared to CLAAS-2.1

The main changes and improvements in the CLAAS-3 algorithms and products compared to the previous edition include:

- A novel probabilistic cloud mask was introduced. The new cloud mask shows overall better agreement with active remote sensing data from the CALIOP instrument. The availability of a cloud probability gives enhanced options for use of the data for specific applications.
- A neural network based algorithm for cloud top height, temperature and pressure was adopted. Compared to CALIOP observations it features in particular an improved height estimate for high clouds.
- For cloud optical and microphysical properties two sets of retrievals are provided: based on the 1.6 and 3.9 μm SEVIRI channels, respectively. In CLAAS-2.1 only 1.6 μm based products were available.
- Liquid cloud droplet number concentration and geometrical thickness are provided as additional cloud properties in the LWP products.
- For all L2 products, except the binary cloud mask and phase, uncertainty estimates are now available, and they are fully propagated into the L3 products. Details on the derivation and propagation of retrieval error estimates can be found in the ATBDs ([RD 2], [RD 3], and [RD 4]).

Finally, the availability of an ICDR, released together with the TCDR and including the same set of products, is also an important improvement in CLAAS-3.

4 Product description

In this section, each cloud product is shortly described regarding retrieval methods, information content and limitations. Validation results are also described shortly for each cloud product, and a summary can be found in Section 5. More details on achieved validation results are given in [RD 1]. At the end of each product description a short statement on recommended application areas is given.

4.1 Fractional cloud cover – CFC

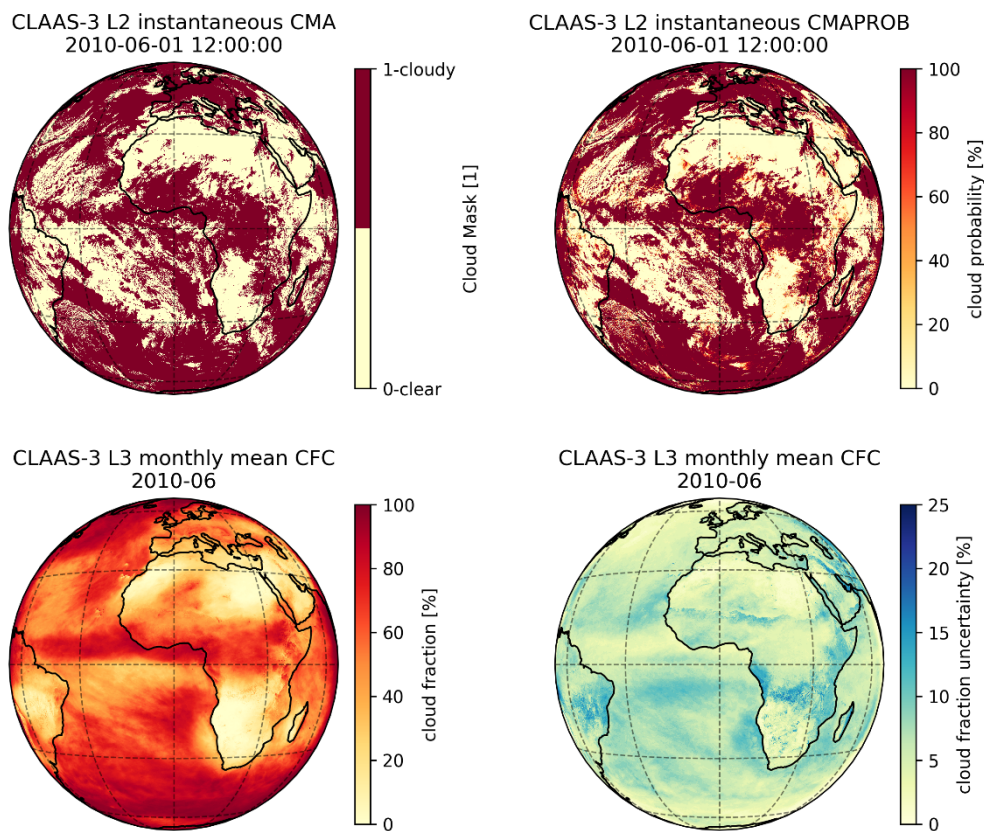



Figure 4-1: CLAAS-3 L2 instantaneous binary cloud mask (top left) and cloud probability (top right) for 1 June 2010 12:00 UTC, and L3 monthly mean cloud fractional cover (bottom left) and the corresponding mean uncertainty for June 2010 (bottom right). Note that the majority of pixels have cloud probabilities close to 0 or 100%, so the top left and right panels look similar.

The L2 (instantaneous pixel) CFC product contains a binary cloud mask and the probabilistic cloud mask. The cloud fractional cover L3 product (monthly and daily mean, as well as monthly mean diurnal cycle) is defined as the fraction of cloudy pixels per grid box compared to the total number of analyzed pixels in the grid box. Pixels are counted as cloudy if the corresponding cloud probability is higher than 50%. Fractional cloud cover is expressed in percent. Examples of L2 binary and probabilistic cloud mask as well as monthly mean CFC and uncertainty are shown in Figure 4-1. Cloud fraction is further separated into low (CTP > 680 hPa), middle (440 hPa < CTP < 680 hPa) and high (CTP < 440 hPa) cloud cover using

	Product User Manual SEVIRI cloud products CLAAS Edition 3	Doc. No: SAF/CM/KNMI/PUM/SEV/CLD Issue: 3.1 Date: 08.08.2022
---	--	--

the CTP product from Section 4.2, as well as daytime (solar zenith angle (SZA) below 75°) and nighttime (SZA above 95°) cloud cover.

Short Algorithm description

The cloud screening and cloud masking is performed using a probabilistic approach (Naïve Bayesian) which is provided by the CMaprob method of an extension to the NWC SAF PPS cloud processing package v2018 [RD 3]. The method is trained using collocations between the CALIPSO-CALIOP cloud lidar and SEVIRI data from Meteosat-9 and Meteosat-10 for the years 2010 and 2015, respectively. The method is an extension (i.e., using several additional spectral channels) of a method originally developed for polar orbiting AVHRR data. Training was performed over different Earth surfaces and sub-divided between day and night. Several ancillary datasets were used (e.g., skin temperatures from ERA5 reanalysis data and surface emissivity maps from MODIS data) to enhance the quality of cloud screening. The training concept means that it is possible to use a threshold of 50 % probability to create a well-balanced binary cloud mask regardless of geographic position. The method is described in detail by Karlsson et al. (2020).

Highlights

- Cloud screening makes optimal use of the multi-channel information from SEVIRI.
- Well-balanced (i.e., neither cloud- or clear-conservative) cloud screening is achieved regardless of underlying Earth surfaces and the time of day. Please see Section 3.2 in [RD 2] for more details, e.g. on surface type definition.
- Daytime conditions with good illumination (i.e, conditions enabling access to information in all spectral channels) provide best cloud screening results.
- Cloud probability means cloud screening with an uncertainty estimation (where 50 % represents maximum uncertainty).

Limitations

- Not all clouds will be detected due to inherent limitations of the SEVIRI imager as being a passive radiometer with a rather coarse field of view (3 x 3 km² at sub-satellite point). This can be compared to actively probing instruments (like cloud lidars and radars) with a much higher cloud detection sensitivity.
- Some thin clouds (particularly, ice clouds) over cold ground surfaces may remain undetected, especially during nighttime. This generally leads to an underestimation of cloud cover.
- The cloud detection algorithm changes from VIS/IR to an infrared only version at the transition from day to night. Some irregularities may occur in the twilight transition zone.
- Since different statistics is used by the method over different Earth surfaces, some artefacts can be seen along coast-lines or major lakes and rivers.

- Since SEVIRI is mounted on geostationary satellites, the well-known dependency of retrieved cloud cover on viewing zenith angle (e.g., Maddux et al., 2010) leads to an overestimation of cloudiness towards the edge of the disk.

Validation

CLAAS-3 CFC was validated in detail with a number of independent data sets in [RD 1]. The results can be summed up as follows. CLAAS-3 and SYNOP observations are in a very good agreement with a small and stable bias of 0.2% in average. CFC was also evaluated against the recently produced Collection 6.1 data from the comparable instrument MODIS which is considered to be the most advanced and best explored passive sensor in space. Averaged over the SEVIRI disk, CLAAS-3 is about 6% lower.

The cloud mask was compared with the space-based lidar instrument CALIOP. The L2 CLAAS-3 cloud mask is in average close to CALIOP, with the Hanssen-Kuipers skill score of 0.7 excluding very thin cloud layers from CALIOP data. The long-term disk average CFC from CLAAS-3 was compared to CALIPSO-GEWEX Level3 cloud product. The bias between the data sets is stable over the whole period. It is negative if thin clouds from CALIPSO are maintained and positive if thin clouds from CALIPSO are excluded.

Near the SEVIRI sub-satellite point MODIS CFC tends to be higher than CLAAS-3, while the opposite is true towards the edge of the disk. This feature was also found in the comparisons with SYNOP data, and is consistent with the expectation that retrieved cloud cover increases with viewing angle.

All long-term comparisons indicate that CLAAS-3 CFC is stable over time (see, for example, the comparison with MODIS in Figure 4-2), although it does feature slight anomalies in the years 2010-2013 and after 2018, which originate from nighttime observations and are most likely related to the calibration of some of the SEVIRI infrared channels (see [RD 1] for more details).

Overall, the CLAAS-3 L2 cloud mask and L3 CFC fulfil the target requirements compared with CALIOP and MODIS, while the L3 CFC product fulfils the optimal requirements (bias less than 5%) with respect to SYNOP.

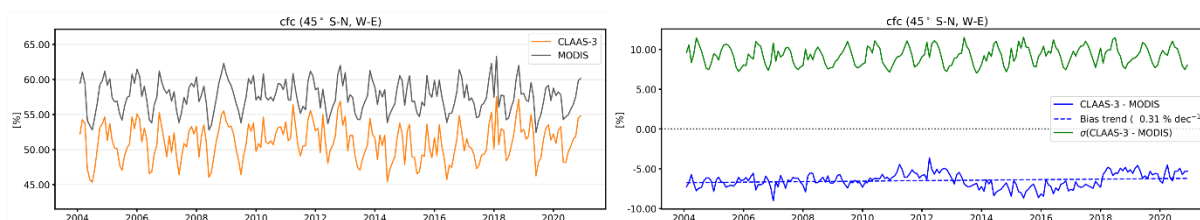


Figure 4-2: Time series of the 45° W-E and S-N area-averaged cloud fractional cover from CLAAS-3 and Aqua MODIS, their biases and the corresponding bc-rmsd. Blue dotted lines in the bias plots show the change in bias (% per decade) based on linear regression.

Recommended applications

The product can be used without restriction, although users should keep in mind that CFC is overestimated at high viewing angles, i.e. towards the edge of the SEVIRI disk. Possible applications of cloud fractional cover are all those which require stable multi-annual and/or spatiotemporally highly resolved CFC values. Tracking of convective cloud systems (Goyens et al., 2011) may serve as an example application here. The cloud mask can also be used as a basis for other retrievals, e.g. of fog (Egli et al., 2018). The CFC product is suitable for the evaluation of regional climate model simulations. As an example, Pfeifroth et al. (2012) evaluated the diurnal cycle of cloud cover in the COSMO-CLM regional climate model using CLAAS-1 data and Ruiz-Arias et al. (2016) evaluated modelled cloud amount over Spain. Studies of the relation between clouds and the underlying land surface have profited from the availability of highly resolved CFC products (Teuling et al., 2017; Garcia-Carreras et al., 2017). Finally, climatological studies of clouds in relation to precipitation and surface irradiance have been facilitated (Alexandri et al., 2017; Hill et al., 2016).

4.2 Cloud Top level – CTO

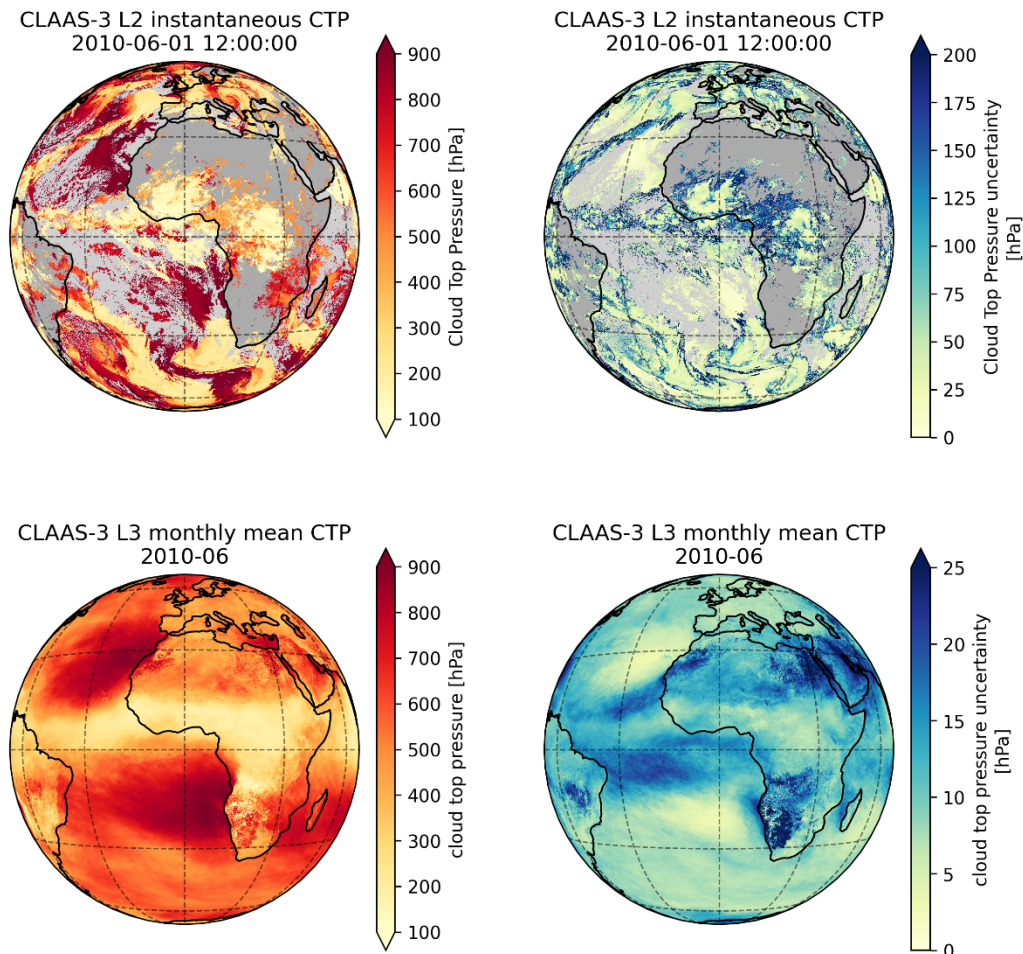



Figure 4-3: CLAAS-3 L2 instantaneous cloud top pressure for 1 June 2010 12:00 UTC (top left) and L3 monthly mean cloud top pressure for June 2010 (bottom left). Corresponding uncertainties are shown on the right.

	Product User Manual SEVIRI cloud products CLAAS Edition 3	Doc. No: SAF/CM/KNMI/PUM/SEV/CLD Issue: 3.1 Date: 08.08.2022
---	--	--

Three versions of the CLAAS Cloud Top product exist:

1. The Cloud Top Temperature (CTT), expressed in Kelvin
2. The Cloud Top Height (CTH), expressed as height (m) above sea level
3. The Cloud Top Pressure (CTP), expressed in hPa

Daily and monthly average products are calculated by averaging the original algorithm output in SEVIRI pixel resolution for all available scenes. All products are averaged arithmetically (linearly) but for the CTP product also a geometric mean (i.e., average of the logarithm of cloud top pressure) is available. Examples of L2 and L3 CTP and their estimated uncertainties are shown in Figure 4-3.

Short Algorithm description

For the determination of cloud top information, the SEVIRI extension to NWC SAF PPS v2018 algorithms is used, details can be found in [RD 3]. The method was originally developed for AVHRR and MODIS data trained with data collocated with CALIPSO-CALIOP measurements (see Håkansson et al., 2018). The algorithm is applied to all cloudy pixels as identified by the binary cloud mask interpreted from cloud probabilities.

The method is a neural network algorithm which uses pre-trained neural networks to predict cloud top pressure. Afterwards, the cloud top temperature and height are derived with the help of NWP auxiliary data (ERA5) for the retrieved pressure.

Highlights

- The method is trained with image features defined for both individual pixels and for pixel surroundings. This has led to greatly enhanced performance compared to previous methods, especially for high-level clouds.
- Cloud top level estimations are enabled for all identified cloudy pixels.
- Uncertainty estimations (16th and 84th percentiles) of the cloud top product are available for all pixels.

Limitations

- Infrared radiation observed by a passive sensor emanates from a certain optical depth within the cloud. In the case of clouds which are optically thin in the upper layers (notably high ice clouds), this typically causes an underestimation of the cloud top height that may amount to several kilometers (e.g., Hamann et al., 2014).
- Clouds are multi-layered in at least 20% of the cases on a global scale. For multi-layered cloud situations, only the top height of the uppermost layer is retrieved. In addition, lower cloud layers usually lead to a negative bias in the retrieval of CTH of the uppermost layer (Hamann et al., 2014).

- The quality of the CTO product depends to some extent on the quality of the reference vertical profiles of temperature and moisture taken from NWP model analyses. Especially troublesome is the treatment of situations with temperature inversions since this implies that there are several solutions to the problem of matching measured cloud top temperatures to vertical reference profiles.

Validation

CLAAS-3 CTO was validated with CALIOP (L2), CALIPSO-GEWEX (L3, CTH only) and compared with MODIS (L2 and L3) observations.

The validation with CALIOP was performed with and without filtering thin upper cloud layers. The validation showed best agreement when the filtering was applied down to an integrated optical depth of around 0.2. In this case CTH and CTP L2 products fulfil the optimum requirements. Without filtering larger differences were obtained. The long-term series of averaged CTH shows no irregularities and a stable bias over the whole time period compared to CALIPSO L3, see Figure 4-4. The slightly better agreement is achieved in comparison with filtered CALIPSO thin clouds (passive flavor).

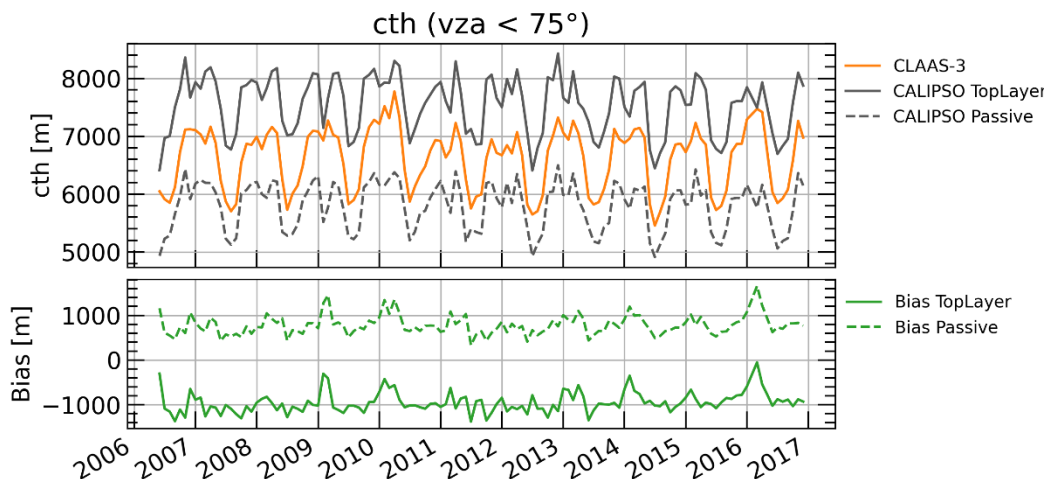



Figure 4-4: Time series of cloud top height (top) and bias (bottom) from CLAAS-3 and CALIPSO-GEWEX top layer and passive flavor; passive flavor is denoted by dashed line.

CLAAS-3 L2 CTH, compared to MODIS L2, shows better agreement of liquid cloud top heights than of ice cloud top heights. In the first case the optimum requirement is fulfilled.

The comparisons with MODIS L3 indicated that the average CTH was higher and CTP lower for CLAAS-3 than for MODIS. The averaged differences are large, so the threshold requirements are missed. However, the biases remain nearly constant over 17 years. Despite of a slight negative trend in CTH, the bias stability of CTH and CTP is within the optimum requirements.

	Product User Manual SEVIRI cloud products CLAAS Edition 3	Doc. No: SAF/CM/KNMI/PUM/SEV/CLD Issue: 3.1 Date: 08.08.2022
---	--	--

Recommended applications

For CTO, similar recommendations as for the CFC products (see Section 4.1) are given, including the applicability at high viewing zenith angles. Possible applications of CTO are those which require stable, multi-annual, and/or spatiotemporally highly resolved CTO values. An example is the height assignment of atmospheric motion vectors (AMVs). Another example is to study the movement of the inter tropical convergence zone (ITCZ) throughout the years or facilitate research on transition from one cloud development stage to another, such as the transition from stratocumulus to cumulus. The product can also be used for the evaluation of regional climate model simulations. As an example, Kuell and Bott (2009) used SEVIRI-derived cloud-top pressure to evaluate a convection parameterization scheme in the COSMO model. Gristey et al. (2018) used CLAAS-2 CTH for the analysis of outgoing longwave radiation with the Met Office model. Finally, Taylor et al. (2017) characterized diurnal cycles of cloud top temperature using CLAAS-2 data.

4.3 Cloud Phase – CPH

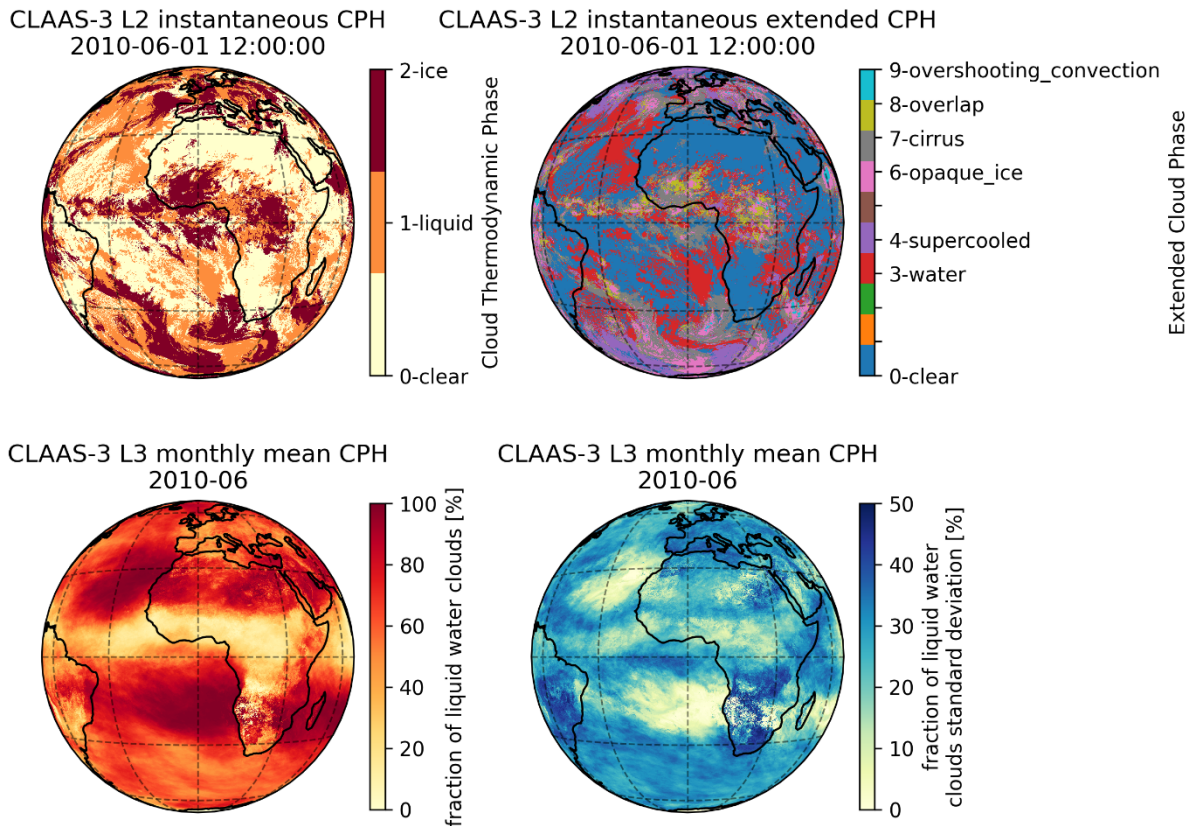


Figure 4-5: CLAAS-3 L2 instantaneous cloud thermodynamic phase (top left) and extended cloud phase (top right) on 1 June 2010 at 12:00 UTC, and L3 monthly mean cloud thermodynamic phase (bottom left) and its mean standard deviation (bottom right) for June 2010.

Short Algorithm description

The cloud phase product is meant to represent the thermodynamic phase of the particles near the cloud top. The cloud-top phase retrieval follows the PATMOS-x algorithm (Heidinger et al., 2013), and is based on a number of threshold tests using SEVIRI channels IR_3.9, IR_6.2, IR_8.7, IR_10.8, IR_12.0, and IR_13.4. Some of the tests involve clear and cloudy-overcast radiances, which are calculated using the Radiative Transfer model for TOVS (RTTOV). The algorithm is run for cloudy pixels and initially yields one of the following cloud types (called 'extended cloud phase'): liquid, supercooled, opaque ice, cirrus, overlap, and overshooting. These are then further condensed to liquid (former two) and ice (latter four) phase. During the subsequent retrieval of cloud optical thickness and particle effective radius the phase may be changed if the shortwave measurements cannot be reconciled with simulated reflectances of clouds with the initially retrieved phase. Therefore, two CPH products exist: cph, consistent with the COT-CRE retrieval using the SEVIRI 3.9 μm channel and cph_16, consistent with the COT-CRE retrieval using the 1.6 μm channel. Obviously, these two flavors can only differ during daytime. More extensive details on the algorithm can be found in [RD 4]. For an example of the (extended) cloud phase see Figure 4-5.

Highlights

- The algorithm provides cloud phase both during daytime and nighttime.
- In addition to liquid/ice discrimination a further breakdown into cloud types is provided.
- The phase discrimination shows good agreement with active CALIOP observations.

Limitations

The main limitations of the CPH retrieval are:

- The identification of thin cirrus over water clouds is challenging.
- Due to the nature of passive satellite observations, the phase near the top of the clouds is retrieved with limited sensitivity to lower cloud layers.

Validation

Thermodynamic phase is evaluated in [RD 1] in terms of the fraction of liquid clouds relative to the total cloud fraction.

The CLAAS-3 CPH product shows a good agreement with CALIOP, with smaller average difference, if the CALIOP phase is taken at an optical depth of 0.2 from above into the cloud. The Hanssen-Kuipers skill score of 0.74 is within the target requirements. If this filtering is not applied, CLAAS-3 has a much larger fraction of liquid clouds than CALIOP.

CPH L3 was also compared with MODIS. The MODIS Infrared (IR) cloud phase product was used, and results from the Terra and Aqua satellites were averaged. CLAAS-3 and MODIS multi-year mean CPH and their differences are shown in Figure 4-6. The CLAAS-3 phase agrees well with the MODIS product, albeit with regional differences. On average, the bias and bc-rmsd of CLAAS-3 phase against MODIS are within the threshold requirements. The bias shows a positive trend, which appears mainly due to a negative trend in MODIS.

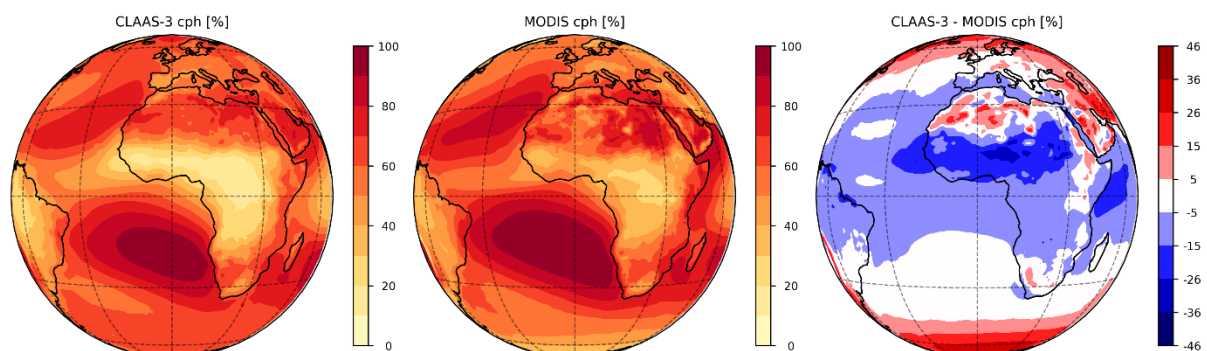


Figure 4-6: CLAAS-3 and MODIS fraction of liquid clouds and their difference averaged from 02/2004 until 12/2020.

Recommended applications

The CPH dataset is specifically useful for studies of cloud development, e.g. convective activity characterized by a transition from liquid to ice phase as the clouds grow vertically (e.g. Bruno et al., 2021, Coopman et al., 2021, and Pan et al., 2021). In general, wherever multi annual, stable and spatiotemporally highly resolved information is needed, CLAAS-3 CPH data may be useful.

4.4 Liquid Water Path – LWP

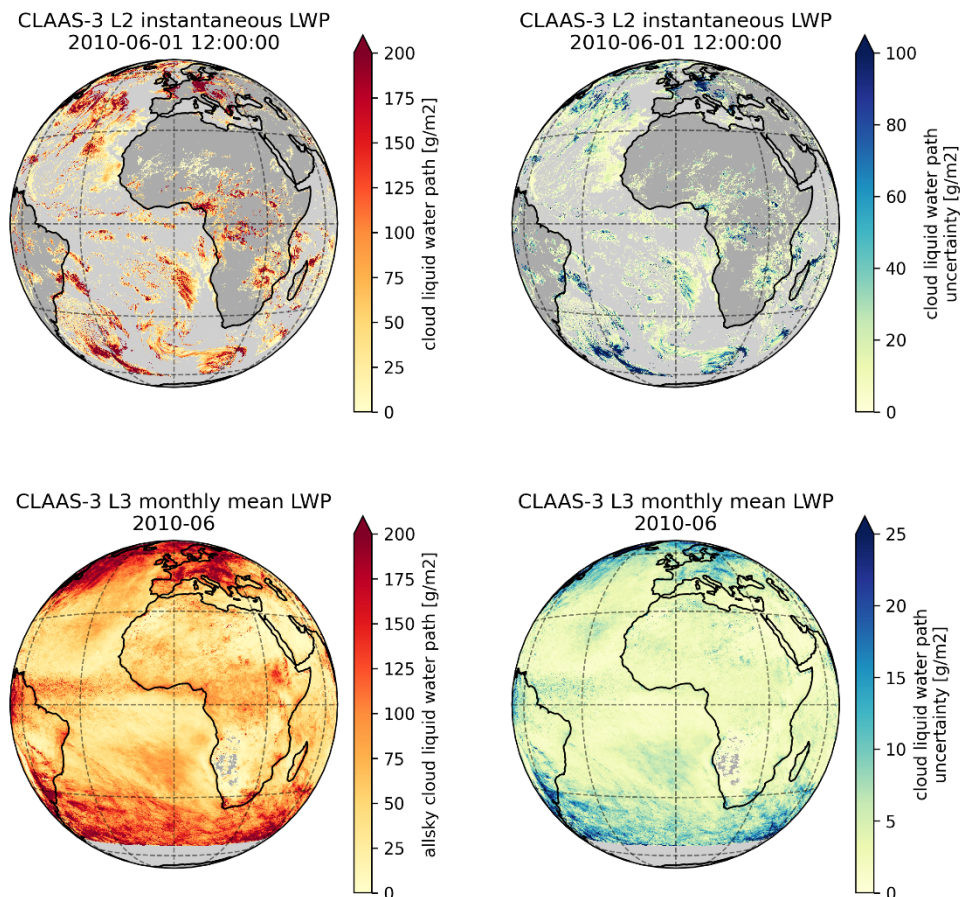



Figure 4-7: CLAAS-3 L2 instantaneous cloud liquid water path on 1 June 2010 at 12:00 UTC (top left) and L3 monthly mean cloud liquid water path for June 2010 (bottom left). Corresponding uncertainties are shown on the right.

Short Algorithm description

The central principle of the method to retrieve cloud optical and microphysical properties is that the reflectance of clouds at a (for cloud particles) non-absorbing wavelength in the visible region (e.g., 0.6 or 0.8 μm) is strongly related to the optical thickness (τ) and has little dependence on particle effective radius (r_e), whereas the reflectance of clouds at an absorbing wavelength in the shortwave-infrared region (e.g., 1.6 or 3.7 μm) is strongly dependent on effective radius (Nakajima and King, 1992).

	Product User Manual SEVIRI cloud products CLAAS Edition 3	Doc. No: SAF/CM/KNMI/PUM/SEV/CLD Issue: 3.1 Date: 08.08.2022
---	--	--

In the CPP algorithm (Benas et al., 2017; Roebeling et al., 2006), the Doubling-Adding KNMI (DAK) radiative transfer model (RTM: De Haan et al., 1987 and Stammes, 2001) is used to simulate 0.6-, and 1.6-, and 3.9- μm top-of-atmosphere reflectances of homogeneous, plane-parallel clouds as a function of viewing and illumination geometry, cloud optical thickness, effective radius, and cloud phase. These simulated reflectances are stored in a look-up table (LUT).

τ and r_e are retrieved for cloudy pixels in an iterative manner by matching satellite-observed reflectances to the LUT of RTM-simulated reflectances. For water clouds effective radii between 3 and 34 μm are retrieved, while τ is limited at 150. From these two properties, the cloud water path (CWP) of water clouds (or liquid water path, LWP) can be computed using the following relation assuming vertically homogeneous liquid water content: (Stephens, 1978):

$$\text{LWP} = 2/3 \rho_l \tau r_e,$$

where ρ_l is the density of liquid water.

Two sets of τ , r_e and LWP are provided: one based on the 0.6-1.6 μm channel combination (suffix _16 in the product files) and one based on the 0.6-3.9 μm channel combination (no suffix). From the latter set of τ and r_e , and now assuming semi-adiabatically stratified clouds, the (vertically constant) cloud droplet number concentration (CDNC) and cloud geometrical thickness (CGT) are derived, following Bennartz and Rausch (2017).

Examples of L2 and L3 LWP products and uncertainties are shown in Figure 4-7.


Highlights

- Together with LWP, τ , r_e , CDNC and CGT are included as additional layers in the L2 and L3 products.
- Estimates of the retrieval errors are provided taking into account a range of error sources.
- The careful calibration of the shortwave SEVIRI channels with MODIS (Meirink et al., 2013) has a pronounced effect on the quality of the retrieved τ and r_e , and thus LWP.

Limitations

The main limitations of the LWP retrieval are:

- The derivation of cloud physical properties from reflected solar radiation is dependent on the availability of daylight. This means that no retrievals can be done during night time. Even if pixel-level retrievals are performed and reported up to solar zenith angles of 84°, for L3 aggregation a maximum SZA of 75° is applied. Similarly, the retrievals become less accurate at very high viewing angles, i.e. near the edge of the disk.
- Sun glint can affect the cloud property retrievals considerably, in particular for broken cloudy scenes over ocean. Therefore, possibly sun glint-affected pixels (defined by a scattering angle differing less than 27 degrees from the direct glint angle) are flagged.
- Cloud property retrievals are performed assuming that clouds are plane parallel. This is true only in a minority of cases, which implies that retrieval errors become larger as

	Product User Manual SEVIRI cloud products CLAAS Edition 3	Doc. No: SAF/CM/KNMI/PUM/SEV/CLD Issue: 3.1 Date: 08.08.2022
---	--	--

clouds deviate from being plane parallel. Especially convective clouds can be problematic, as they frequently have illuminated and shadowed sides (see, e.g., Marshak et al. 2006). Broken and sub-pixel cloud fields, including cloud edges, can also cause problems for retrieving cloud properties, since a passive satellite sensor measures an averaged radiance of the cloudy and cloud-free part of a pixel. The error made in these cases is among others dependent on the contrast between clouds and underlying surface, the true properties of the cloud, and the cloud fraction within the sampling resolution of the instrument (Coakley et al. 2005).

- The retrieval is highly problematic over very bright surfaces, particularly ice and snow, as the visible reflectance from clouds is similar to that from the surface. To enable the user to filter these potentially problematic cases, information about highly reflecting surfaces is included in the L2 CPP files (*processing_flag*, see Section 7.1.3.3) and in the L3 LWP and IWP files (*high_surfbalbedo_fraction*, see Sections 7.2.3.4 and 7.2.3.5, respectively).
- Unlike active satellite instruments, which can derive cloud profile information, retrievals from passive satellite instruments are limited by the fact that the obtained signal emanates from the integrated profile. Since near-infrared radiation is only penetrating into the cloud to a certain depth (due to absorption by cloud particles), the retrieved effective radius is representative for the upper part of the cloud (Platnick 2001). The penetration depth depends on the amount of absorption by cloud particles, which is increasing with wavelength. This means that the retrieved CPH and r_e depend on which NIR spectral channel is used (in our case 1.6 or 3.9 μm).
- Aerosols are not considered in the CPP retrieval. This assumption is usually justified because aerosols reside below or within the cloud and their optical thickness is small compared to that of the cloud. However, if the aerosols reside above the cloud and if they are sufficiently absorbing, they can significantly lower the visible reflectance. The effect on the retrievals depends on the channel combination used and on the aerosol properties. This leads to underestimations of both τ and r_e , and thus LWP (Haywood et al. 2004).

Validation

The CLAAS-3 LWP product is evaluated in [RD 1] with passive microwave observations (L2 AMSR2 data and the MAC-LWP L3 dataset) as well as with MODIS. The comparisons with MAC-LWP focus on a region in the south Atlantic dominated by stratocumulus fields. For this region, CLAAS-3 LWP is on average consistent with the microwave based data, both in terms of seasonal and diurnal cycle.

Validation of CLAAS-3 LWP with AMSR2 shows overall modest biases and bc-rmsd, fulfilling the target requirements.

The comparison with MODIS is illustrated in Figure 4-8, showing that LWP spatial distributions agree well. CLAAS-3 all-sky LWP has higher values than MODIS mainly in higher latitudes and secondarily in the stratocumulus region of the southeast Atlantic. Note, that difference patterns vary between the retrievals based on the 3.9 μm and 1.6 μm channel, more details in [RD 1]. The CLAAS-3 and MODIS time series are in very good agreement in both channel pair

retrievals, in terms of both seasonality patterns and absolute values. The bias and the bias stability fulfil the optimal requirements.

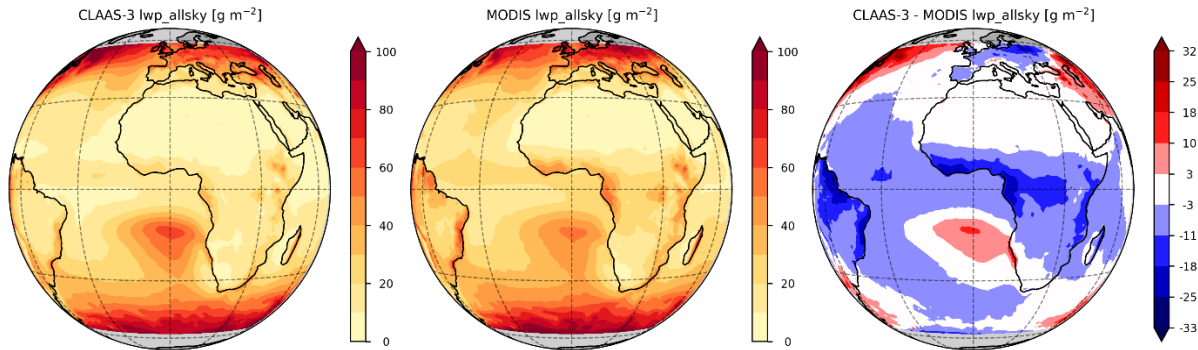


Figure 4-8: CLAAS-3 and MODIS all-sky liquid water path retrieved based on the 3.9 μm channel and their difference averaged from 02/2004 until 12/2020.

Recommended applications

The LWP dataset is most reliable at lower latitudes, or (better said) lower solar zenith angles (below about 65 degrees). In addition, high latitudes are frequently affected by snow and ice cover, making it difficult to estimate cloud optical properties against the bright background. Retrievals also become more uncertain towards the edge of the disk in west and east direction, where viewing angles become large, causing increased sensitivity to deviations of clouds from the plane parallel assumption.

In general, use of LWP is recommended where multi annual, stable and spatiotemporally highly resolved information is needed. An important application is the evaluation of cloud water path, optical thickness and effective radius in regional weather and climate models (e.g., Alexandri et al., 2015; Greuell et al., 2011; Roebeling and van Meijgaard, 2009). Seethala et al. (2018) characterized the diurnal cycle of stratocumulus clouds in the southeast Atlantic with various satellite datasets. Finally, LWP and related cloud properties can be used for process studies. For example, Fuchs et al. (2017) investigated the impact of air mass origin on the properties of low clouds in the southeast Atlantic using CLAAS-2 data.

4.5 Ice Water Path – IWP

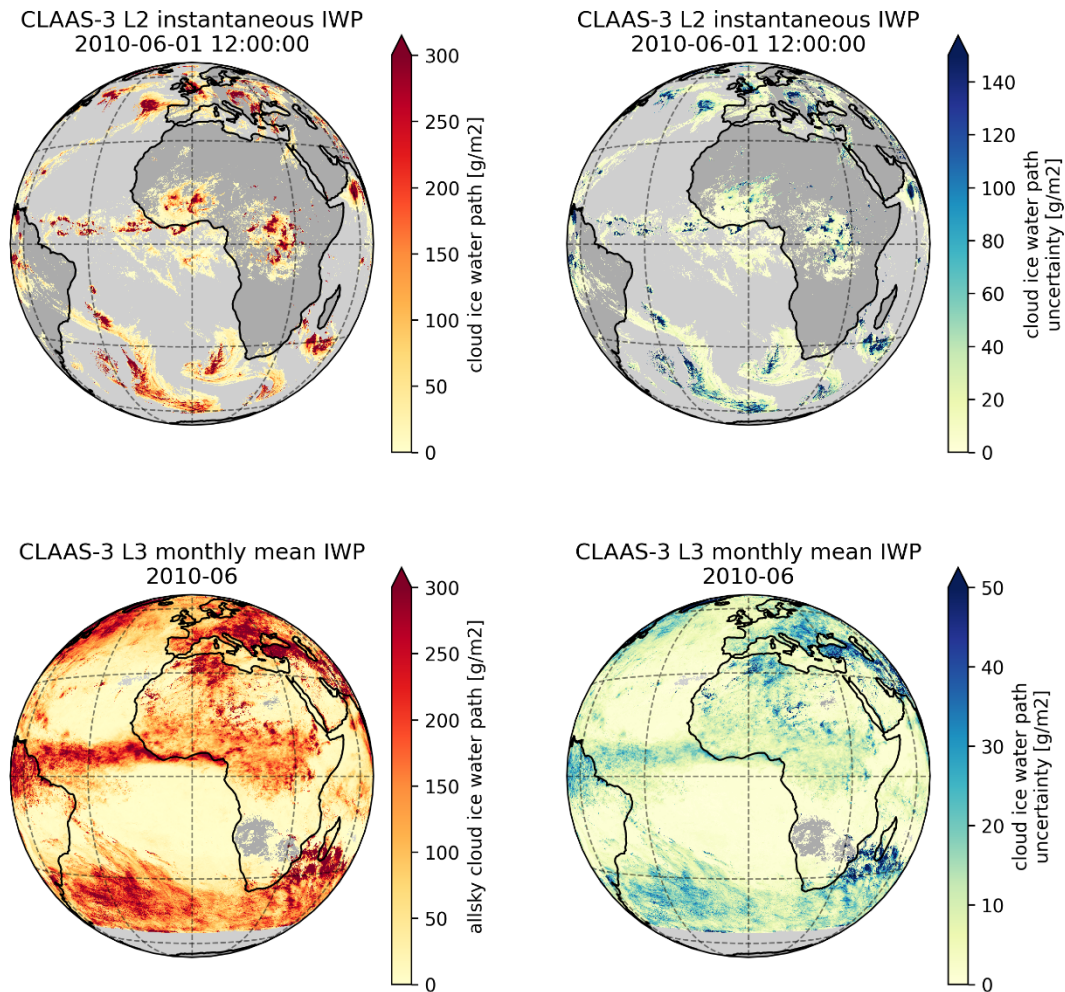


Figure 4-9: CLAAS-3 L2 instantaneous cloud ice water path on 1 June 2010 at 12:00 UTC (top left) and L3 monthly mean cloud ice water path for June 2010 (bottom left). Corresponding uncertainties are shown on the right.

Short Algorithm description

Ice water path is retrieved in the same way as LWP but with τ and r_e retrievals based on RTM simulations for collections of severely roughened aggregated solid columns (Yang et al., 2013 and Baum et al., 2011) with effective radii ranging between 5 and 60 μm .

Examples of L2 and L3 IWP products and uncertainties are shown in Figure 4-9.

Highlights

The highlights mentioned for LWP also hold for IWP.

Limitations

The same limitations as for LWP hold also for IWP. In addition, the τ and especially r_e retrieval for ice clouds is considerably more uncertain than for water clouds, because particle shapes and roughness vary widely and are not well known. The assumptions on ice crystal habits used to generate the LUTs have a profound impact on the retrieved r_e and IWP. Retrievals of multi-layer clouds are problematic. Typically, a scene with cirrus overlying low liquid water clouds will be assigned the ice phase, and the retrieved COT and IWP will include contributions from both cloud layers.

Validation

The CLAAS-3 IWP product is evaluated in [RD 1] with DARDAR observations for L2 as well as with MODIS for L3.

Compared with DARDAR, the CLAAS-3 IWP is on average negatively biased. CLAAS-3 products tend to overestimate IWP of thin clouds and underestimate IWP of thick clouds. These biases originate both from the optical thickness and the effective radius. The latter is considerably smaller in CLAAS-3 than in DARDAR (for which a weighted average of the profile near the cloud top was used as a reference), and shows very low correlation. Comparisons with MODIS also show that the CLAAS-3 ice CRE is somewhat smaller.

Multi-year mean spatial distributions and area-averaged time series of CLAAS-3 all-sky IWP were compared with MODIS. As for LWP there is a very good agreement in the spatial patterns, especially over the ocean, see Figure 4-10. CLAAS-3 IWP is overall slightly higher than MODIS IWP.

The long-term series of CLAAS and MODIS IWP agree very well, with overall slightly higher CLAAS-3 values, and small differences between 1.6 μm and 3.9 μm retrievals. The bias and the bias stability are within the optimal requirements.

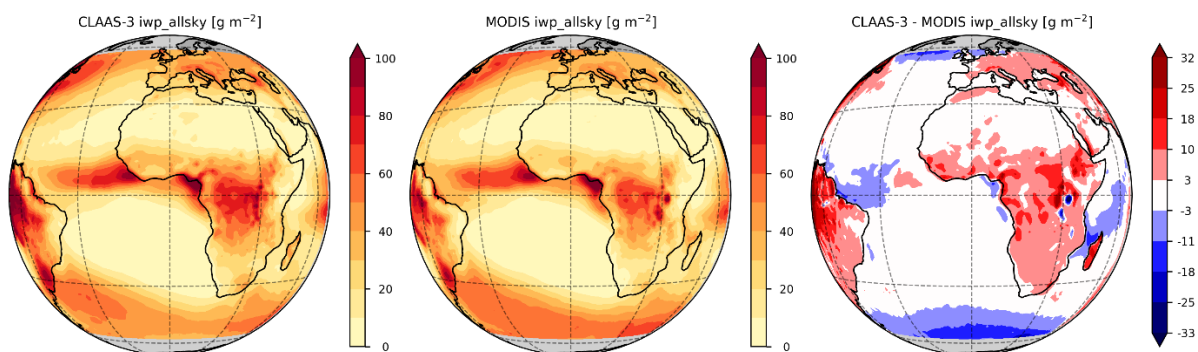


Figure 4-10: CLAAS-3 and MODIS all-sky ice water path path retrieved based on the 3.9 μm channel and its difference averaged from 02/2004 until 12/2020.

Recommended applications

The IWP dataset is just like LWP most reliable where solar and viewing zenith angles are not too high (below about 65 degrees). Use of CLAAS-3 IWP is recommended where multi annual, stable and spatiotemporally highly resolved information is needed. IWP has regularly been applied for model evaluation and process studies. Rybka et al. (2021) used CLAAS-2 IWP for the analysis of large-eddy simulations of summer convection. Nickovic et al. (2016) evaluated ice nucleation parameterizations with IWP data. Roebeling and van Meijgaard (2009) assessed the diurnal cycle of cloud water path, as simulated by a regional climate model over Europe.

4.6 Joint Cloud property Histogram – JCH

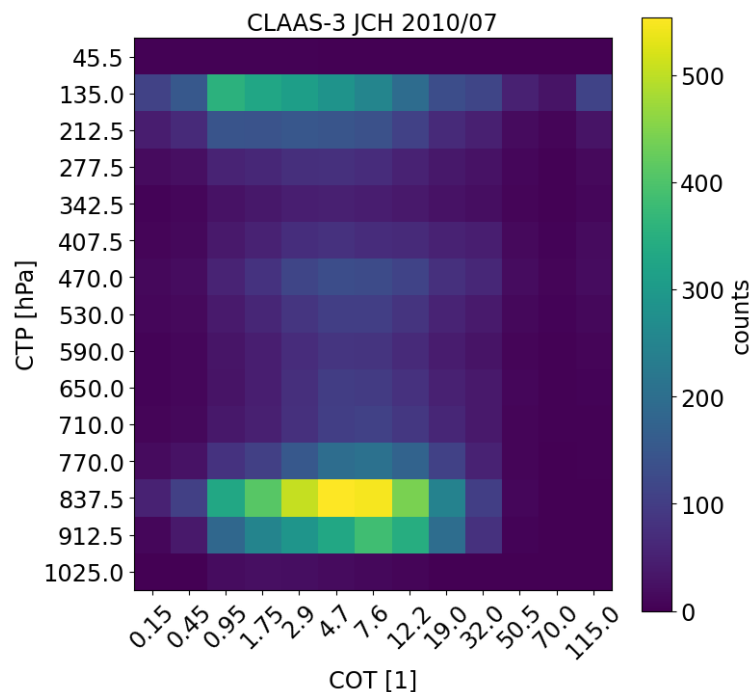


Figure 4-11: JCH, a 2D histogram of cloud top pressure and cloud optical thickness, here aggregated over the 45° S-N, W-E area for 07/2010.

Short Algorithm description

The JCH product is a combined histogram of CTP and COT covering the solution space of both parameters. This two-dimensional histogram gives the absolute number of occurrences of COT and CTP combinations defined by specific bins. It is further separated in liquid and ice clouds. An example of JCH (for liquid plus ice clouds) for July 2010 is shown in Figure 4-11.

Highlights

- The product adds value to the single standard L3 products of CTP and COT by showing how the two parameters vary together.
- Supports cloud regimes/types analyses.
- The use of joint histograms is common in applications for evaluating climate models.
- The CLAAS-3 COT and CTP bins for the JCH product have been chosen such that they are a superset of the traditional ISCCP bins. Thus, the CLAAS-3 product can be aggregated to exactly the same bins as used for the ISCCP product.

Limitations

- The product is only available during daytime since the COT parameter is not retrieved at night.

Recommended applications

The JCH product is compiled as distributions for each spatial grid cell, thus it is possible to compose cloud distribution statistics for any region size on the globe by simple aggregation of grid point values. As an example, the CLAAS-1 JCH was used by Van Weverberg et al. (2012) to evaluate model-simulated cloud properties.

As mentioned above the JCH product can be used for cloud regime/type analyses. Figure 4-12 and Figure 4-13 show the results of an exemplary application, for which the JCH histograms of all Junes in 2005 to 2020 have been aggregated per grid cell, and then been clustered over all grid cells using k-means clustering (MacQueen, 1967). The number of clusters is generally flexible but set to six in this example. Figure 4-12 shows the cluster each grid cell is assigned to. Figure 4-13 shows the centroid JCH for each cluster. It should be noted that monthly JCH might span a too long time period for some applications. Daily JCH products, although not being official products, are available on request from the CM SAF help desk.

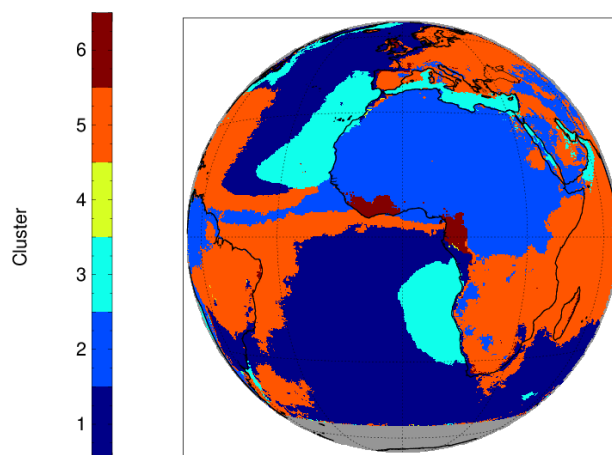


Figure 4-12: Map showing the number of the cluster (see Figure 4-13) each grid cell is assigned to.

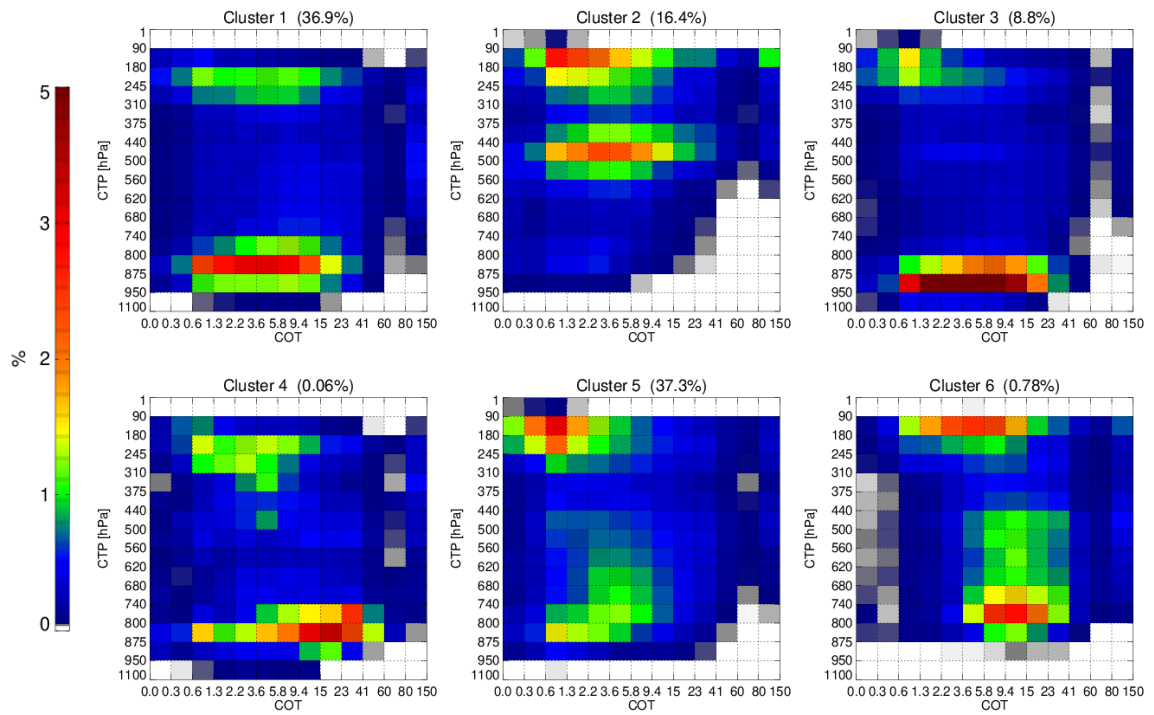



Figure 4-13: Centroid JCH for each of the six clusters, after being scaled by its total number to represent relative frequency of each COT-CTP bin. Also given are the portions of all grid cells belonging to each cluster.

5 Summary table of validation results regarding product accuracy


Table 5-1 shows the achieved accuracies of the cloud products as discussed in [RD 1]. The acronyms used are: SYNOP = Synoptical surface observations, CALIOP = Cloud-Aerosol Lidar with Orthogonal Polarisation, MODIS = Moderate Resolution Imaging Spectroradiometer, AMSR2 = Advanced Microwave Scanning Radiometer 2, MAC-LWP Multisensor Advanced Climatology of Liquid Water Path., and DARDAR = raDAR/liDAR. All references are described in detail in [RD 1].

Table 5-1: Summary of CLAAS-3 validation results compared to requirements for each cloud product. Required and achieved accuracies are formulated in terms of bias, precisions in terms of bc-rmsd (except for CFC and CPH L2, for which the metric is the Hanssen-Kuipers Skill Score, KSS), and stabilities in terms of decadal trend in bias. All numbers, except KSS, are in the units indicated for the respective cloud products. Validation results are color-coded as follows: **worse than threshold**, **fulfils threshold**, **fulfils target**, and **fulfils optimal** requirement. CALIOP results are reported for different values of (I)COT, the cloud optical thickness integrated from the top of the cloud. Evaluations against MODIS are indicated in grey since they are viewed as consistency checks rather than true validation. CPH, LWP and IWP validation scores are for the 3.9- μ m-based products.

L2 or L3	Reference	Accuracy (bias)		Precision (bc-rmsd)		Stability (decadal trend in bias)	
		Req'd (target)	Ach'd	Req'd (target)	Ach'd	Req'd (target)	Ach'd
Cloud Fractional Cover (CFC) [%]							
L2	CALIOP (COT > 0)			0.6 (KSS)	0.67		
	CALIOP (COT > 0.2)				0.70		
L3	SYNOP	5	0.2	10	8.9	2	0.5
	CALIOP (COT>0)		-2.3		22.5		-0.8
	CALIOP (COT \geq 0.3)		5.8		21.0		-1.5
	MODIS		-6.5		9.2		0.3
Cloud Top Height (CTH) [m]							
L2	CALIOP (ICOT > 0)	800	-1015	2400	3032		
	CALIOP (ICOT > 0.2)		230		2260		
	MODIS (liquid)		17		1175		
	MODIS (ice)		911		1224		
L3	CALIOP (ICOT > 0)	800	-951	1600	3319	270	178
	CALIOP (ICOT \geq 0.3)		780		3044		73
	MODIS		2263		1625		-37
Cloud Top Pressure (CTP) [hPa]							
L2	CALIOP (ICOT > 0)	45	42	135	150		
	CALIOP (ICOT > 0.2)		-15		119		
L3	MODIS	45	-167	90	90	15	3.1
Cloud Phase (CPH), defined as fraction of liquid clouds [%]							
L2	CALIOP (ICOT > 0)			0.6 (KSS)	0.70		
	CALIOP (ICOT > 0.2)				0.74		
L3	MODIS	5	-5.9	10	13.2	2	2.4

	Product User Manual SEVIRI cloud products CLAAS Edition 3	Doc. No: SAF/CM/KNMI/PUM/SEV/CLD Issue: 3.1 Date: 08.08.2022
---	--	--

Liquid Water Path (LWP) [g m ⁻²]							
L2	AMSR2	10	0.1	50	49		
	MODIS		-15		84		
L3	MAC-LWP	10	0.3	20	11.4	3	1.6
	MODIS		-4.0		10.8		0.2
Ice Water Path (IWP) [g m ⁻²]							
L2	DARDAR v3.00	20	-58	100	277		
	DARDAR v3.10		-29		227		
	MODIS		-36		168		
L3	MODIS	20	1.5	40	17.9	6	0.1
Joint Cloud property Histogram (JCH)							
L3		n/a		n/a		n/a	

	Product User Manual SEVIRI cloud products CLAAS Edition 3	Doc. No: SAF/CM/KNMI/PUM/SEV/CLD Issue: 3.1 Date: 08.08.2022
---	--	--

6 Summary and outlook

In this report the characteristics of the CM SAF CLAAS-3 data record have been described. CLAAS-3 consists of a TCDR, covering the years 2004 to 2020, and an ICDR, which is the continuous and consistent extension of the data record into the present. An overview of the various cloud products was given, consisting of brief retrieval algorithm descriptions, inventories of the main benefits and limitations, summaries of the main validation results, and recommendations for usage of the data.

CLAAS-3 provides a wealth of information on cloud properties at high spatial and temporal resolution, making it useful for a range of applications including model evaluation and process studies. With its length, 17 years for the TCDR, and continuously growing with the ICDR, it is also becoming of increasing interest for climate studies.

In CDOP 4 (the next phase of the CM SAF project) a follow-up version of the CLAAS data record will be produced. The experience that we gained while creating and evaluating the current edition will be incorporated into the next dataset version.

New features in CLAAS-4 will likely include:

- The applied algorithms will be updated after a careful testing of performance and quality. In particular, a new neural network based cloud phase scheme is foreseen.
- The calibration of the SEVIRI measurements will be re-assessed using developments at EUMETSAT and in the Global Space-Based Inter-Calibration System (GSICS) project. In particular for the infrared channels improvements are expected.
- The new series of EUMETSAT geostationary satellites – Meteosat Third Generation (MTG) carrying the Flexible Combined Imager (FCI) – will be seamlessly integrated in the data record.

The CALIPSO and CloudSat datasets were found to deliver very valuable information both for algorithm development and for the analysis and validation of CLAAS-3 L2 products. This role will be taken over by the EarthCARE mission, which is currently planned to be launched in 2023.

7 Data format description

CLAAS-3 products are provided as NetCDF-4 (Network Common Data Format v4) files (<http://www.unidata.ucar.edu/software/netcdf/>) with internal compression. The data files are created following NetCDF Climate and Forecast (CF) Metadata Convention version 1.7 (<http://cf-pcmdi.llnl.gov/>) and NetCDF Attribute Convention for Dataset Discovery version 1.3.

For data processing and conversion to various graphical packages input format, CM SAF recommends the usage of the climate data operators (CDO), available under GNU Public License (GPL) from MPI-M (<http://www.mpimet.mpg.de/cdo>).

7.1 Data format description of non-averaged products

L2 data are stored in the native satellite projection. The corresponding lat/lon grid is available in a separate auxiliary file, see Section 7.1.5.

7.1.1 General variables

CLAAS-3 L2 data is provided on a grid of 3712 x 3712 pixels, excluding a number of space pixels at the edge of the SEVIRI full disk.

Table 7-1 lists the general variables which are used in all L2 products.

Table 7-1: General variables in each L2 product.

Name	Description
<i>time</i>	observation timestamp in days since 1970-01-01 00:00 UTC
<i>time_bnds</i>	two-dimensional array reporting the actual temporal coverage of the observation for each timestamp in variable <i>time</i>
<i>georef_offset_corrected</i>	flag indicates if the correction due to the data shift against the nominal GEOS projection is applied (SEVIRI L1.5 data is shifted by 1.5 km SSP North and West until December 2017)
<i>projection</i>	projection information
<i>platform_flag</i>	MSG number
Satellite position:	
- <i>subsatellite_alt</i>	- actual satellite altitude
- <i>subsatellite_lat</i>	- actual satellite latitude
- <i>subsatellite_lon</i>	- actual satellite longitude
<i>record_status</i>	overall status of each record in the file: 0: "ok", 1: "void", 2: "bad_quality"

7.1.2 Common attributes

The data fields provide a set of general attributes, which are listed and described in Table 7-2. Bold attributes are mandatory for each non-coordinate variable. If available, a *standard_name* is provided.

Table 7-2: Common attributes of each variable in L2 data.

Name	Description
<i>_FillValue</i>	This number represents missing or undefined data. Missing values are to be filtered before applying scale factor and offset
<i>valid_range</i>	Specifies the valid range of the data [min,max]
<i>long_name</i>	Long descriptive name of the variable
<i>standard_name</i>	Standard name that references a description of a variable's content in the CF standard name table
<i>scale_factor</i>	The data are to be multiplied by this factor after it is read
<i>add_offset</i>	This number is to be added to the data after it is read. If <i>scale_factor</i> is present, it has to be applied first.
<i>units</i>	Physical unit
<i>flag_values</i> , <i>flag_masks</i> , <i>flag_meanings</i>	These attributes describe variables containing status flags. The <i>flag_values/flag_masks</i> attributes describe all possible values of the status flag, whereas <i>flag_meanings</i> indicates the meaning of a certain flag value. See section 3.5 in the CF standard for details.
<i>cell_methods</i>	describes the aggregation method for the <i>time</i> axis (here <i>point</i> = instantaneous value)

If *scale_factor* or *add_offset* are present, the data have been scaled. To obtain the physical value *p* of a variable *v*, multiply it by *scale_factor* and add *add_offset* afterwards:

$$p = scale_factor * v + add_offset$$

7.1.3 Product specific data fields

This section provides a detailed description of each variable in the CLAAS-3 L2 products. Please note that we use the FORTRAN-like dimension order here. The *ncdump* utility, for example, displays the dimensions in reversed (C-like) order. The column (longitude direction) dimension is denoted with *x* and the line (latitude direction) dimension with *y*. Both are equal to 3712, while the time dimension in L2 files is equal to 1.

7.1.3.1 Cloud mask (CMA)

cma(x, y, time)

binary cloud mask

cma_prob(x, y, time)

probabilistic cloud mask

status_flag(x, y, time)

status flag for probabilistic cloud mask, incl. surface categories

quality(x, y, time)

retrieval flag

conditions(x, y, time)

geophysical and processing conditions flags

7.1.3.2 Cloud top (CTX)

ctt(x, y, time)

cloud top temperature

ctp(x, y, time)

cloud top pressure

cth(x, y, time)

cloud top height

quality(x, y, time)

retrieval flag

conditions(x, y, time)

geophysical and processing conditions flag

7.1.3.3 Cloud physical properties (CPP)

cph(x, y, time)

cloud phase based on the 0.6 – 3.9 μm retrieval

cph_16(x, y, time)

cloud phase based on the 0.6 – 1.6 μm retrieval

cwp(x, y, time)

cloud water path (LWP or IWP) based on the 0.6 – 3.9 μm retrieval

cwp_16(x, y, time)

cloud water path (LWP or IWP) based on the 0.6 – 1.6 μm retrieval

cot(x, y, time)

cloud optical thickness based on the 0.6 – 3.9 μm retrieval

cot_16(x, y, time)

cloud optical thickness based on the 0.6 – 1.6 μm retrieval

cre(x, y, time)

droplet / ice particle effective radius based on the 0.6 – 3.9 μm retrieval

cre_16(x, y, time)

droplet / ice particle effective radius based on the 0.6 – 1.6 μm retrieval

cdnc(x, y, time)

cloud droplet number concentration based on the 0.6 – 3.9 μm retrieval

cgt(x, y, time)

geometrical thickness of a liquid water cloud based on the 0.6 – 3.9 μm retrieval

cwp_unc(x, y, time)

retrieval error in CWP based on the 0.6 – 3.9 μm retrieval

cwp_16_unc(x, y, time)

retrieval error in CWP based on the 0.6 – 1.6 μm retrieval

cot_unc(x, y, time)

retrieval error in COT based on the 0.6 – 3.9 μm retrieval


cot_16_unc(x, y, time)

retrieval error in COT based on the 0.6 – 1.6 μm retrieval

cre_unc(x, y, time)

retrieval error in CRE based on the 0.6 – 3.9 μm retrieval

cre_16_unc(x, y, time)

	Product User Manual SEVIRI cloud products CLAAS Edition 3	Doc. No: SAF/CM/KNMI/PUM/SEV/CLD Issue: 3.1 Date: 08.08.2022
---	--	--

retrieval error in CRE based on the 0.6 – 1.6 μm retrieval

$h_sigma(x, y, time)$

relative standard deviation of the visible reflectances

$processing_flag(x, y, time)$


retrieval quality flag

7.1.4 Global attributes


Each L2 NetCDF file also possesses general attributes that are valid for all variables contained in this file. These attributes are described in Table 7-3.

Table 7-3: General attributes of a non-averaged NetCDF file.

Name	Description
<i>comment</i>	Data in this file are stored in SEVIRI image coordinates. Please visit the DOI page to obtain the corresponding Lat-Lon grid.
<i>id</i>	DOI:10.5676/EUM_SAF_CM/CLAAS/V003
<i>product_version</i>	3.0
<i>creator_name</i>	DE/DWD
<i>creator_email</i>	contact.cmsaf@dwd.de
<i>creator_url</i>	https://www.cmsaf.eu/
<i>institution</i>	EUMETSAT/CM SAF
<i>project</i>	Satellite Application Facility on Climate Monitoring (CM SAF)
<i>references</i>	https://doi.org/10.5676/EUM_SAF_CM/CLAAS/V003
<i>platform</i>	Earth Observation Satellites > METEOSAT > METEOSAT-8/-9/-10/-11
<i>instrument</i>	Earth Remote Sensing Instruments>Passive Remote Sensing >Spectrometers/Radiometers>Imaging Spectrometers/Radiometers>SEVIRI>Spinning Enhanced Visible and Infrared Imager
<i>time_coverage_start</i>	Temporal coverage start of the data [ISO8601 date]
<i>time_coverage_end</i>	Temporal coverage end of the data [ISO8601 date]
<i>time_coverage_duration</i>	Temporal coverage duration of the data [ISO8601 date]

	Product User Manual SEVIRI cloud products CLAAS Edition 3	Doc. No: SAF/CM/KNMI/PUM/SEV/CLD Issue: 3.1 Date: 08.08.2022
---	--	--

Name	Description
<i>geospatial_lat_min*</i>	-81.2 / -81.07
<i>geospatial_lat_max*</i>	81.2 / 81.07
<i>geospatial_lat_units</i>	degrees_north
<i>geospatial_lon_min*</i>	-81.26 / -81.13
<i>geospatial_lon_max*</i>	81.26 / 81.13
<i>geospatial_lon_units</i>	degrees_east
<i>keywords</i>	EARTH SCIENCE>ATMOSPHERE>CLOUDS>"variable group"
<i>Conventions</i>	convention tables for metadata and attributes (CF-1.7, ACDD-1.3)
<i>keywords_vocabulary</i>	Vocabulary for keywords in the global attributes (GCMD Science Keywords, Version 8.6)
<i>standard_name_vocabulary</i>	Vocabulary for standard names in the parameter attributes (Standard Name Table (v70, 10 December 2019))
<i>instrument_vocabulary</i>	Vocabulary for the instrument in the global attributes (GCMD Instruments, Version 8.6)
<i>platform_vocabulary</i>	Vocabulary for the platform in the global attributes (GCMD Platforms, Version 8.6)
<i>date_created</i>	Point in time, when the file was created [ISO8601 date]
<i>CMSAF_area</i>	cmsaf_disk
<i>CMSAF_proj4_params</i>	Projection parameters for PROJ.4 library
<i>CMSAF_area_extent*</i>	Projection coordinates of the area corners in meters [lower left x, lower left y, upper right x, upper right y]
<i>CMSAF_L2_processor</i>	NWC/PPS version v2018 patch5 + CmsafPpsSeviri 0.5.0
<i>CMSAF_reprocessing_software</i>	claas-v3.0
<i>license</i>	The CM SAF data are owned by EUMETSAT and are available to all users free of charge and with no conditions to use. If you wish to use these products, EUMETSAT's copyright credit must be shown by displaying the words "Copyright (c) (2022) EUMETSAT" under/in each of these SAF Products used in a project or shown in a publication or website.

	Product User Manual SEVIRI cloud products CLAAS Edition 3	Doc. No: SAF/CM/KNMI/PUM/SEV/CLD Issue: 3.1 Date: 08.08.2022
---	--	--

Name	Description
	Please follow the citation guidelines given at https://doi.org/10.5676/EUM_SAF_CM/CLAAS/V003 and also register as a user at http://cm-saf.eumetsat.int/ to receive latest information on CM SAF services and to get access to the CM SAF User Help Desk.
<i>variable_id</i>	names of the main variables in the product

* *area extent is adjusted due to the shift against the nominal GEOS projection*

7.1.5 Auxiliary data

The CLAAS-3 L2 dataset goes along with a set of auxiliary data. Because the SEVIRI disk and its viewing geometry are (quasi) constant with time, there is no need to include auxiliary information into the product files. Instead, this information is included in a separate file, which is available via the DOI webpage. The contents of the file are listed in Table 7-4.

The additional dimension *georef_offset_corrected* in spatially resolved variables denotes the correction of the SEVIRI L1.5 data shift by 1.5km SSP North and West against the nominal GEOS projection until December 2017. *georef_offset_corrected* flag is provided in each CLAAS-3 L2 product to allow matching the auxiliary data properly.

Table 7-4: Contents of the file with auxiliary data, named *claas3_level2_aux_data.nc*.

Name	Description
<i>georef_offset_corrected</i>	flag indicates if the correction due to the data shift against the nominal GEOS projection is applied
<i>lat(georef_offset_corrected, x, y)</i>	latitude
<i>lon(georef_offset_corrected, x, y)</i>	longitude
<i>acq_time(georef_offset_corrected, x, y)</i>	scanline acquisition time relative to scan start
<i>lsm(georef_offset_corrected, x, y)</i>	land sea mask
<i>alt(georef_offset_corrected, x, y)</i>	altitude above geoid
<i>pixel_area(georef_offset_corrected, x, y)</i>	surface area covered by each pixel
<i>lon0</i>	set of most prominent subsatellite points
<i>satzen(georef_offset_corrected, x, y, lon0)</i>	satellite zenith angle
subsatellite points for different MSGs:	
- <i>msg1_lon0_id</i>	- subsatellite points occupied by MSG1

Name	Description
- <i>msg2_lon0_id</i>	- subsatellite points occupied by MSG2
- <i>msg3_lon0_id</i>	- subsatellite points occupied by MSG3
- <i>msg4_lon0_id</i>	- subsatellite points occupied by MSG4
occupation duration of subsatellite points:	
- <i>msg1_lon0_time_bounds</i>	- occupation duration of MSG1 subsatellite points
- <i>msg2_lon0_time_bounds</i>	- occupation duration of MSG2 subsatellite points
- <i>msg3_lon0_time_bounds</i>	- occupation duration of MSG3 subsatellite points
- <i>msg4_lon0_time_bounds</i>	- occupation duration of MSG4 subsatellite points

7.2 Monthly and daily mean data file contents

A common NetCDF file consists of dimensions, variables, and attributes. These components can be used together to capture the meaning of data and relations among data. All CLAAS-3 product files are built following the same design principles. The averaged data are provided as daily and monthly means and as mean diurnal cycle. For the latter all time slots within one hour are averaged to a daily mean diurnal cycle. All diurnal cycles of a month are averaged to the monthly mean diurnal cycle. The daily means are based on all available time slots. The monthly mean is an average of all daily means. The product files contain general variables, which are common for all files, and product specific variables. The latter are three-dimensional, except for the histograms. Dimensions of all three-dimensional fields are named *time*, *lon*, *lat*. For the JCHs, additionally two dimensions for COT and CTP bins are included. All other provided histograms have one additional dimension for variable bins. The CPH L3 products contain three-dimensional averaged fields as well as four-dimensional histogram fields.

General variables of each file are summarized in Table 7-5. All data fields, which are described in section 7.2.3, also contain specific attributes as given in section 7.2.2. Global attributes of each file are reported in section 7.2.4.

7.2.1 General variables

CLAAS-3 L3 data is provided on a regular grid with a spatial resolution of $0.05^\circ \times 0.05^\circ$ degrees for monthly averages, and $0.25^\circ \times 0.25^\circ$ for the Joint Cloud property Histogram and the monthly mean diurnal cycle fields. Table 7-5 presents the general variables which are used in all L3 products.

Table 7-5: General variables in each L3 product.

Name	Description
<i>time</i>	start of averaging/composite time period; In case of diurnal cycles, this vector has 24 elements [days counted from 1970-01-01]
<i>time_bnds</i>	two-dimensional array defining the averaging/composite time period
<i>lat</i>	geographical latitude of grid-box centre [degree_north]
<i>lon</i>	geographical longitude of grid-box centre [degree_east]
<i>record_status</i>	overall status of each record in the file: 0: "ok", 1: "void", 2: "bad_quality"

7.2.2 Common attributes

Table 7-6 summarizes the attributes which are assigned to each data field in the NetCDF files. Keep in mind that, depending on the parameter, some attributes can be omitted, for example if no standard name is defined.

Table 7-6: Attributes assigned to each variable in L3 data.

Name	Description
<i>_FillValue</i>	This number represents missing or undefined data. Missing values are to be filtered before scaling.
<i>valid_min</i>	smallest valid value of a variable
<i>valid_max</i>	largest valid value of a variable
<i>long_name</i>	long descriptive name
<i>standard_name</i>	standard name that references a description of a variable's content in the CF standard name table
<i>scale_factor</i>	The data are to be multiplied by this factor after it is read.
<i>add_offset</i>	This number is to be added to the data after it is read. If <i>scale_factor</i> is present, the data are first scaled before the offset is added.
<i>units</i>	physical unit

7.2.3 Product specific data fields

This section provides a detailed description of each variable in the CLAAS-3 L3 products. Please note that we use the FORTRAN-like dimension order here. The *ncdump* utility for example, displays the dimensions in reversed (C-like) order.

7.2.3.1 Fractional cloud coverage (CFC)

nobs(lon, lat, time)

number of observations used to create mean CFC

nobs_day(lon, lat, time)

number of observations used to create mean daytime CFC

nobs_night(lon, lat, time)

number of observations used to create mean night-time CFC

cfc(lon, lat, time)

mean CFC value given in percent

cfc_std(lon, lat, time)

standard deviation over all CFC data points

cfc_unc_mean(lon, lat, time)

mean of CFC uncertainty given in percent

cfc_day(lon, lat, time)

mean daytime CFC value given in percent

cfc_night(lon, lat, time)

mean nighttime CFC value given in percent

cfc_low(lon, lat, time)

mean CFC of all clouds with CTP larger than 680 hPa given in percent

cfc_middle(lon, lat, time)

mean CFC of all clouds with CTP between 440hPa and 680 hPa given in percent

cfc_high(lon, lat, time)

mean CFC of all clouds with CTP smaller than 440 hPa given in percent

cma_prob(lon, lat, time)


mean probabilistic CFC value given in percent

cma_prob_day(lon, lat, time)

mean probabilistic daytime CFC value given in percent

cma_prob_night(lon, lat, time)

mean probabilistic night-time CFC value given in percent

	Product User Manual SEVIRI cloud products CLAAS Edition 3	Doc. No: SAF/CM/KNMI/PUM/SEV/CLD Issue: 3.1 Date: 08.08.2022
---	--	--

7.2.3.2 Cloud phase (CPH)

nobs(lon, lat, time)

number of observations available for CPH

nobs_cloud(lon, lat, time)

number of observations used to create mean CPH based on 0.6 – 3.9 μm retrieval

nobs_cloud_16(lon, lat, time)

number of observations used to create mean CPH based on 0.6 – 1.6 μm retrieval

nobs_cloud_day(lon, lat, time)

number of observations used to create mean daytime CPH based on 0.6 – 3.9 μm retrieval

nobs_cloud_16_day(lon, lat, time)

number of observations used to create mean daytime CPH based on 0.6 – 1.6 μm retrieval

cph(lon, lat, time)

mean liquid cloud fraction based on 0.6 – 3.9 μm retrieval given in percent

cph_16(lon, lat, time)

mean liquid cloud fraction based on 0.6 – 1.6 μm retrieval given in percent

cph_std(lon, lat, time)

standard deviation over all CPH data points based on 0.6 – 3.9 μm retrieval

cph_16_std(lon, lat, time)

standard deviation over all CPH data points based on 0.6 – 1.6 μm retrieval

cph_day(lon, lat, time)

mean daytime liquid cloud fraction based on 0.6 – 3.9 μm retrieval given in percent

cph_16_day(lon, lat, time)

mean daytime liquid cloud fraction based on 0.6 – 1.6 μm retrieval given in percent

cph_day_std(lon, lat, time)

standard deviation over all daytime CPH data point based on 0.6 – 3.9 μm retrieval

cph_16_day_std(lon, lat, time)

standard deviation over all daytime CPH data points based on 0.6 – 1.6 μm retrieval

hist1d_cph_bin_centre(hist1d_cph_bin_centre)

vector contains centre of extended cloud phase bins. Ten extended cloud phase bins are: clear, _, _, water, supercooled, _, opaque_ice, cirrus, overlap, overshooting_convection.

hist1d_cph(lon, lat, hist1d_cph_bin_centre, time)

number of observations of each extended cloud phase at given spatial location for values based on 0.6 – 3.9 μm retrieval

hist1d_cph(lon, lat, hist1d_cph_bin_centre, time)

number of observations of each extended cloud phase at given spatial location for values based on 0.6 – 1.6 μm retrieval

7.2.3.3 Cloud top level (CTO)

nobs(lon, lat, time)

number of available observations

nobs_cloud(lon, lat, time)

number of cloudy classified observations used to create mean cloud top products

nobs_cloud_day_liq(lon, lat, time)

number of observations used to create mean cloud top products for liquid clouds at day

nobs_cloud_day_ice(lon, lat, time)

number of observations used to create mean cloud top products for ice clouds at day

nobs_cloud_night_liq(lon, lat, time)

number of observations used to create mean cloud top products for liquid clouds at night

nobs_cloud_night_ice(lon, lat, time)

number of observations used to create mean cloud top products for ice clouds at night

cth(lon, lat, time)

arithmetical mean cloud top height (CTH)

cth_liq_day(lon, lat, time)

arithmetical mean CTH for liquid clouds at day

cth_liq_night(lon, lat, time)

arithmetical mean CTH for liquid clouds at night

cth_ice_day(lon, lat, time)

arithmetical mean CTH for ice clouds at day

cth_ice_night(lon, lat, time)

arithmetical mean CTH for ice clouds at night

cth_std(lon, lat, time)

standard deviation over CTH data points

cth_unc01(lon, lat, time)

CTH uncertainty assuming correlation of 0.1

cth_unc10(lon, lat, time)

CTH uncertainty assuming correlation of 1.0

cth_unc_mean(lon, lat, time)

CTH uncertainty mean

cth_unc2_mean(lon, lat, time)

CTH squared uncertainty mean

cth_unc_std(lon, lat, time)

standard deviation over CTH uncertainty data points

ctp(lon, lat, time)

arithmetical mean cloud top pressure (CTP)

ctp_liq_day(lon, lat, time)

arithmetical mean CTP for liquid clouds at day

ctp_liq_night(lon, lat, time)

arithmetical mean CTP for liquid clouds at night

ctp_ice_day(lon, lat, time)

arithmetical mean CTP for ice clouds at day

ctp_ice_night(lon, lat, time)

arithmetical mean CTP for ice clouds at night

ctp_std(lon, lat, time)

standard deviation over CTP data points

ctp_unc01(lon, lat, time)

CTP uncertainty assuming correlation of 0.1

ctp_unc10(lon, lat, time)

CTP uncertainty assuming correlation of 1.0

ctp_unc_mean(lon, lat, time)

CTP uncertainty mean

ctp_unc2_mean(lon, lat, time)

CTP squared uncertainty mean

ctp_unc_std(lon, lat, time)

standard deviation over CTP uncertainty data points

ctp_log(lon, lat, time)

logarithmic mean CTP

ctt(lon, lat, time)

arithmetical mean cloud top temperature (CTT)

ctt_liq_day(lon, lat, time)

arithmetical mean CTT for liquid clouds at day

ctt_liq_night(lon, lat, time)

arithmetical mean CTT for liquid clouds at night

ctt_ice_day(lon, lat, time)

arithmetical mean CTT for ice clouds at day

ctt_ice_night(lon, lat, time)

arithmetical mean CTT for ice clouds at night

ctt_std(lon, lat, time)

standard deviation over CTT data points

ctt_unc01(lon, lat, time)

CTT uncertainty assuming correlation of 0.1

ctt_unc10(lon, lat, time)

CTT uncertainty assuming correlation of 1.0

ctt_unc_mean(lon, lat, time)


CTT uncertainty mean

ctt_unc2_mean(lon, lat, time)

CTT squared uncertainty mean

ctt_unc_std(lon, lat, time)

standard deviation over CTT uncertainty data points

	Product User Manual SEVIRI cloud products CLAAS Edition 3	Doc. No: SAF/CM/KNMI/PUM/SEV/CLD Issue: 3.1 Date: 08.08.2022
---	--	--

7.2.3.4 Liquid water path (LWP)

nobs(lon, lat, time)

number of available observations used to create mean LWP

nobs_cloud_cot_liq(lon, lat, time)

number of observations used to create mean LWP and liquid COT based on 0.6 – 3.9 μm retrieval

nobs_cloud_cot_16_liq(lon, lat, time)

number of observations used to create mean LWP and liquid COT based on 0.6 – 1.6 μm retrieval

nobs_cloud_cre_liq(lon, lat, time)

number of observations used to create mean liquid CRE, CDNC and CGT based on 0.6 – 3.9 μm retrieval

nobs_cloud_cre_16_liq(lon, lat, time)

number of observations used to create mean liquid CRE, based on 0.6 – 1.6 μm retrieval

SZA(lon, lat, time)

mean solar zenith angle of successful retrieval results and liquid phase results

SZA_std(lon, lat, time)

standard deviation of the solar zenith angle of successful retrieval results and liquid phase results

lwp(lon, lat, time)

mean LWP based on 0.6 – 3.9 μm retrieval


lwp_allsky(lon, lat, time)

grid box mean LWP based on 0.6 – 3.9 μm retrieval, weighted by the grid box cloud fraction

lwp_std(lon, lat, time)

standard deviation of the LWP based on 0.6 – 3.9 μm retrieval

lwp_unc01(lon, lat, time)

	Product User Manual SEVIRI cloud products CLAAS Edition 3	Doc. No: SAF/CM/KNMI/PUM/SEV/CLD Issue: 3.1 Date: 08.08.2022
---	--	--

LWP uncertainty assuming correlation of 0.1, based on 0.6 – 3.9 μm retrieval

lwp_unc10(lon, lat, time)

LWP uncertainty assuming correlation of 1.0, based on 0.6 – 3.9 μm retrieval

lwp_unc_mean(lon, lat, time)

mean LWP retrieval error based on 0.6 – 3.9 μm retrieval

lwp_unc2_mean(lon, lat, time)

squared mean LWP retrieval error based on 0.6 – 3.9 μm retrieval

lwp_unc_std(lon, lat, time)

standard deviation of the LWP retrieval error based on 0.6 – 3.9 μm retrieval

lwp_16(lon, lat, time)

mean LWP based on 0.6 – 1.6 μm retrieval

lwp_16_allsky(lon, lat, time)

grid box mean LWP based on 0.6 – 1.6 μm retrieval, weighted by the grid box cloud fraction

lwp_16_std(lon, lat, time)

standard deviation of the LWP based on 0.6 – 1.6 μm retrieval

lwp_16_unc01(lon, lat, time)

LWP uncertainty assuming correlation of 0.1, based on 0.6 – 1.6 μm retrieval

lwp_16_unc10(lon, lat, time)

LWP uncertainty assuming correlation of 1.0, based on 0.6 – 1.6 μm retrieval

lwp_16_unc_mean(lon, lat, time)

mean LWP retrieval error based on 0.6 – 1.6 μm retrieval

lwp_16_unc2_mean(lon, lat, time)

squared mean LWP retrieval error based on 0.6 – 1.6 μm retrieval

lwp_16_unc_std(lon, lat, time)

standard deviation of the LWP retrieval error based on 0.6 – 1.6 μm retrieval

cot_liq(lon, lat, time)

mean liquid cloud optical thickness (COT) based on 0.6 – 3.9 μm retrieval

cot_liq_log(lon, lat, time)

logarithmic mean liquid COT

cot_liq_std(lon, lat, time)

standard deviation of the liquid COT based on 0.6 – 3.9 μm retrieval

cot_liq_unc01(lon, lat, time)

liquid COT uncertainty assuming correlation of 0.1, based on 0.6 – 3.9 μm retrieval

cot_liq_unc10(lon, lat, time)

liquid COT uncertainty assuming correlation of 1.0, based on 0.6 – 3.9 μm retrieval

cot_liq_unc_mean(lon, lat, time)

mean liquid COT retrieval error based on 0.6 – 3.9 μm retrieval

cot_liq_unc2_mean(lon, lat, time)

squared mean liquid COT retrieval error based on 0.6 – 3.9 μm retrieval

cot_liq_unc_std(lon, lat, time)

standard deviation of the liquid COT retrieval error based on 0.6 – 3.9 μm retrieval

cot_16_liq(lon, lat, time)

mean liquid COT based on 0.6 – 1.6 μm retrieval

cot_16_liq_log(lon, lat, time)

logarithmic mean liquid COT

cot_16_liq_std(lon, lat, time)

standard deviation of the liquid COT based on 0.6 – 1.6 μm retrieval

cot_16_liq_unc01(lon, lat, time)

liquid COT uncertainty assuming correlation of 0.1, based on 0.6 – 1.6 μm retrieval

cot_16_liq_unc10(lon, lat, time)

liquid COT uncertainty assuming correlation of 1.0, based on 0.6 – 1.6 μm retrieval

cot_16_liq_unc_mean(lon, lat, time)

mean liquid COT retrieval error based on 0.6 – 1.6 μm retrieval

cot_16_liq_unc2_mean(lon, lat, time)

squared mean liquid COT retrieval error based on 0.6 – 1.6 μm retrieval

cot_16_liq_unc_std(lon, lat, time)

standard deviation of the liquid COT retrieval error based on 0.6 – 1.6 μm retrieval

cre_liq(lon, lat, time)

mean effective radius of liquid droplets (CRE) based on 0.6 – 3.9 μm retrieval

cre_liq_std(lon, lat, time)

standard deviation of the liquid CRE based on 0.6 – 3.9 μm retrieval

cre_liq_unc01(lon, lat, time)

liquid CRE uncertainty assuming correlation of 0.1, based on 0.6 – 3.9 μm retrieval

cre_liq_unc10(lon, lat, time)

liquid CRE uncertainty assuming correlation of 1.0, based on 0.6 – 3.9 μm retrieval

cre_liq_unc_mean(lon, lat, time)

mean liquid CRE retrieval error based on 0.6 – 3.9 μm retrieval

cre_liq_unc2_mean(lon, lat, time)

squared mean liquid CRE retrieval error based on 0.6 – 3.9 μm retrieval

cre_liq_unc_std(lon, lat, time)

standard deviation of the liquid CRE retrieval error based on 0.6 – 3.9 μm retrieval

cre_16_liq(lon, lat, time)

mean liquid CRE based on 0.6 – 1.6 μm retrieval

cre_16_liq_std(lon, lat, time)

standard deviation of the liquid CRE based on 0.6 – 1.6 μm retrieval

cre_16_liq_unc01(lon, lat, time)

liquid CRE uncertainty assuming correlation of 0.1, based on 0.6 – 1.6 μm retrieval

cre_16_liq_unc10(lon, lat, time)

liquid CRE uncertainty assuming correlation of 1.0, based on 0.6 – 1.6 μm retrieval

cre_16_liq_unc_mean(lon, lat, time)

mean liquid CRE retrieval error based on 0.6 – 1.6 μm retrieval

cre_16_liq_unc2_mean(lon, lat, time)

squared mean liquid CRE retrieval error based on 0.6 – 1.6 μm retrieval

cre_16_liq_unc_std(lon, lat, time)

standard deviation of the liquid CRE retrieval error based on 0.6 – 1.6 μm retrieval

cdnc_liq(lon, lat, time)

mean cloud droplet number concentration of liquid clouds (CDNC) based on 0.6 – 3.9 μm retrieval

cdnc_liq_std(lon, lat, time)

standard deviation of the CDNC based on 0.6 – 3.9 μm retrieval

cdnc_liq_unc01(lon, lat, time)

CDNC uncertainty assuming correlation of 0.1, based on 0.6 – 3.9 μm retrieval

cdnc_liq_unc10(lon, lat, time)

CDNC uncertainty assuming correlation of 1.0, based on 0.6 – 3.9 μm retrieval

cdnc_liq_unc_mean(lon, lat, time)

mean CDNC retrieval error based on 0.6 – 3.9 μm retrieval

cdnc_liq_unc2_mean(lon, lat, time)

squared mean CDNC retrieval error based on 0.6 – 3.9 μm retrieval

cdnc_liq_unc_std(lon, lat, time)

standard deviation of the CDNC retrieval error based on 0.6 – 3.9 μm retrieval


cgt_liq(lon, lat, time)

mean geometrical thickness of liquid clouds (CGT) based on the 0.6 – 3.9 μm retrieval

cgt_liq_std(lon, lat, time)

standard deviation of the CGT based on 0.6 – 3.9 μm retrieval

cgt_liq_unc01(lon, lat, time)

	Product User Manual SEVIRI cloud products CLAAS Edition 3	Doc. No: SAF/CM/KNMI/PUM/SEV/CLD Issue: 3.1 Date: 08.08.2022
---	--	--

CGT uncertainty assuming correlation of 0.1, based on 0.6 – 3.9 μm retrieval

cgt_liq_unc10(lon, lat, time)

CGT uncertainty assuming correlation of 1.0, based on 0.6 – 3.9 μm retrieval

cgt_liq_unc_mean(lon, lat, time)

mean CGT retrieval error based on 0.6 – 3.9 μm retrieval

cgt_liq_unc2_mean(lon, lat, time)

squared mean CGT retrieval error based on 0.6 – 3.9 μm retrieval

cgt_liq_unc_std(lon, lat, time)

standard deviation of the CGT retrieval error based on 0.6 – 3.9 μm retrieval

h_sigma_liq_mean(lon, lat, time)

mean scene heterogeneity computed for liquid clouds

h_sigma_liq_std(lon, lat, time)

standard deviation of scene heterogeneity computed for liquid clouds

high_surfalbedo_fraction(lon, lat, time)

fractional occurrence of high surface albedo, most frequently due to snow cover or sea ice

7.2.3.5 Ice water path (IWP)

nobs(lon, lat, time)

number of available observations used to create mean IWP

nobs_cloud_cot_ice(lon, lat, time)


number of observations used to create mean IWP and ice COT based on 0.6 – 3.9 μm retrieval

nobs_cloud_cot_16_ice(lon, lat, time)

number of observations used to create mean IWP and ice COT based on 0.6 – 1.6 μm retrieval

nobs_cloud_cre_ice(lon, lat, time)

number of observations used to create mean ice CRE

	Product User Manual SEVIRI cloud products CLAAS Edition 3	Doc. No: SAF/CM/KNMI/PUM/SEV/CLD Issue: 3.1 Date: 08.08.2022
---	--	--

based on 0.6 – 3.9 μm retrieval

nobs_cloud_cre_16_ice(lon, lat, time)

number of observations used to create mean ice CRE, based on 0.6 – 1.6 μm retrieval

SZA(lon, lat, time)

mean solar zenith angle of successful retrieval results and ice phase results

SZA_std(lon, lat, time)

standard deviation of the solar zenith angle of successful retrieval results and ice phase results

iwp(lon, lat, time)

mean IWP based on 0.6 – 3.9 μm retrieval

iwp_allsky(lon, lat, time)

grid box mean IWP based on 0.6 – 3.9 μm retrieval, weighted by the grid box cloud fraction

iwp_std(lon, lat, time)

standard deviation of the IWP based on 0.6 – 3.9 μm retrieval

iwp_unc01(lon, lat, time)

IWP uncertainty assuming correlation of 0.1, based on 0.6 – 3.9 μm retrieval

iwp_unc10(lon, lat, time)

IWP uncertainty assuming correlation of 1.0, based on 0.6 – 3.9 μm retrieval

iwp_unc_mean(lon, lat, time)

mean IWP retrieval error based on 0.6 – 3.9 μm retrieval

iwp_unc2_mean(lon, lat, time)

squared mean IWP retrieval error based on 0.6 – 3.9 μm retrieval

iwp_unc_std(lon, lat, time)

standard deviation of the IWP retrieval error based on 0.6 – 3.9 μm retrieval

iwp_16(lon, lat, time)

mean IWP based on 0.6 – 1.6 μm retrieval

iwp_16_allsky(lon, lat, time)

grid box mean IWP based on 0.6 – 1.6 μm retrieval, weighted by the grid box cloud fraction

iwp_16_std(lon, lat, time)

standard deviation of the IWP based on 0.6 – 1.6 μm retrieval

iwp_16_unc01(lon, lat, time)

IWP uncertainty assuming correlation of 0.1, based on 0.6 – 1.6 μm retrieval

iwp_16_unc10(lon, lat, time)

IWP uncertainty assuming correlation of 1.0, based on 0.6 – 1.6 μm retrieval

iwp_16_unc_mean(lon, lat, time)

mean IWP retrieval error based on 0.6 – 1.6 μm retrieval

iwp_16_unc2_mean(lon, lat, time)

squared mean IWP retrieval error based on 0.6 – 1.6 μm retrieval

iwp_16_unc_std(lon, lat, time)

standard deviation of the IWP retrieval error based on 0.6 – 1.6 μm retrieval

cot_ice(lon, lat, time)

mean ice cloud optical thickness (COT) based on 0.6 – 3.9 μm retrieval

cot_ice_log(lon, lat, time)

logarithmic mean ice COT

cot_ice_std(lon, lat, time)

standard deviation of the ice COT based on 0.6 – 3.9 μm retrieval

cot_ice_unc01(lon, lat, time)

ice COT uncertainty assuming correlation of 0.1, based on 0.6 – 3.9 μm retrieval

cot_ice_unc10(lon, lat, time)

ice COT uncertainty assuming correlation of 1.0, based on 0.6 – 3.9 μm retrieval

cot_ice_unc_mean(lon, lat, time)

mean ice COT retrieval error based on 0.6 – 3.9 μm retrieval

cot_ice_unc2_mean(lon, lat, time)

squared mean ice COT retrieval error based on 0.6 – 3.9 μm retrieval

cot_ice_unc_std(lon, lat, time)

standard deviation of the ice COT retrieval error based on 0.6 – 3.9 μm retrieval

cot_16_ice(lon, lat, time)

mean ice COT based on 0.6 – 1.6 μm retrieval

cot_16_ice_log(lon, lat, time)

logarithmic mean ice COT

cot_16_ice_std(lon, lat, time)

standard deviation of the ice COT based on 0.6 – 1.6 μm retrieval

cot_16_ice_unc01(lon, lat, time)

ice COT uncertainty assuming correlation of 0.1, based on 0.6 – 1.6 μm retrieval

cot_16_ice_unc10(lon, lat, time)

ice COT uncertainty assuming correlation of 1.0, based on 0.6 – 1.6 μm retrieval

cot_16_ice_unc_mean(lon, lat, time)

mean ice COT retrieval error based on 0.6 – 1.6 μm retrieval

cot_16_ice_unc2_mean(lon, lat, time)

squared mean ice COT retrieval error based on 0.6 – 1.6 μm retrieval

cot_16_ice_unc_std(lon, lat, time)

standard deviation of the ice COT retrieval error based on 0.6 – 1.6 μm retrieval

cre_ice(lon, lat, time)

mean effective radius of ice particles (CRE) based on 0.6 – 3.9 μm retrieval

cre_ice_std(lon, lat, time)

standard deviation of the ice CRE based on 0.6 – 3.9 μm retrieval

cre_ice_unc01(lon, lat, time)

ice CRE uncertainty assuming correlation of 0.1, based on 0.6 – 3.9 μm retrieval

cre_ice_unc10(lon, lat, time)

ice CRE uncertainty assuming correlation of 1.0, based on 0.6 – 3.9 μm retrieval

cre_ice_unc_mean(lon, lat, time)

mean ice CRE retrieval error based on 0.6 – 3.9 μm retrieval

cre_ice_unc2_mean(lon, lat, time)

squared mean ice CRE retrieval error based on 0.6 – 3.9 μm retrieval

cre_ice_unc_std(lon, lat, time)

standard deviation of the ice CRE retrieval error based on 0.6 – 3.9 μm retrieval

cre_16_ice(lon, lat, time)

mean ice CRE based on 0.6 – 1.6 μm retrieval

cre_16_ice_std(lon, lat, time)

standard deviation of the ice CRE based on 0.6 – 1.6 μm retrieval

cre_16_ice_unc01(lon, lat, time)

ice CRE uncertainty assuming correlation of 0.1, based on 0.6 – 1.6 μm retrieval

cre_16_ice_unc10(lon, lat, time)

ice CRE uncertainty assuming correlation of 1.0, based on 0.6 – 1.6 μm retrieval

cre_16_ice_unc_mean(lon, lat, time)

mean ice CRE retrieval error based on 0.6 – 1.6 μm retrieval

cre_16_ice_unc2_mean(lon, lat, time)

squared mean ice CRE retrieval error based on 0.6 – 1.6 μm retrieval

cre_16_ice_unc_std(lon, lat, time)

standard deviation of the ice CRE retrieval error based on 0.6 – 1.6 μm retrieval

h_sigma_ice_mean(lon, lat, time)

mean scene heterogeneity computed for ice clouds

h_sigma_ice_std(lon, lat, time)

standard deviation of scene heterogeneity computed for ice clouds

high_surfalbedo_fraction(lon, lat, time)

fractional occurrence of high surface albedo, most frequently due to snow cover or sea ice

7.2.3.6 Joint Cloud property Histograms (JCH)

hist_phase(hist_phase)

two-elements vector containing liquid and ice phase

hist2d_cot_bin_border(hist_cot_bin_border)

vector contains outer limits of the COT bins

hist2d_cot_bin_centre(hist_cot_bin_centre)

vector contains centre of the COT bins

hist2d_ctp_bin_border(hist_ctp_bin_border)

vector contains outer limits of the CTP bins

hist2d_ctp_bin_centre(hist_ctp_bin_centre)

vector contains centre of the CTP bins

cfc(lon, lat, time)

mean fractional cloud cover, used to the JCH

hist2d_cot_ctp(lon, lat, hist2d_cot_bin_centre, hist2d_ctp_bin_centre, hist_phase, time)

number of occurrences of specific combinations of COT and CTP ranges at given spatial location. The Joint Cloud property Histograms are defined on coarser spatial resolution (0.25°) compared to all other products.

7.2.3.7 One-dimensional histograms

Cloud top histograms

hist_phase(hist_phase)

two-elements vector containing liquid and ice phase

hist1d_ctt_bin_border(hist_ctt_bin_border)

vector contains outer limits of the CTT bins

hist1d_ctt_bin_centre(hist_ctt_bin_centre)

vector contains centre of the CTT bins

hist1d_ctp_bin_border(hist_ctp_bin_border)

vector contains outer limits of the CTP bins

hist1d_ctp_bin_centre(hist_ctp_bin_centre)

vector contains centre of the CTP bins

hist1d_ctt(lon, lat, hist1d_ctt_bin_centre, hist_phase, time)

number of occurrences of specific CTT ranges at given spatial location.

hist1d_ctp(lon, lat, hist1d_ctp_bin_centre, hist_phase, time)

number of occurrences of specific CTP ranges at given spatial location.

Cloud water path histograms (includes LWP and IWP histograms)

hist_phase(hist_phase)

two-elements vector containing liquid and ice phase

hist1d_cwp_bin_border(hist_cwp_bin_border)

vector contains outer limits of the cloud water path (CWP) bins

hist1d_cwp_bin_centre(hist_cwp_bin_centre)

vector contains centre of the CWP bins

hist1d_cot_bin_border(hist_cot_bin_border)

vector contains outer limits of the cloud optical thickness (COT) bins

hist1d_cot_bin_centre(hist_cot_bin_centre)

vector contains centre of the COT bins


hist1d_cre_bin_border(hist_cre_bin_border)

vector contains outer limits of the cloud particle effective radius (CRE) bins

hist1d_cre_bin_centre(hist_cre_bin_centre)

vector contains centre of the REF bins

hist1d_cdnc_bin_border(hist_cdnc_bin_border)

	Product User Manual SEVIRI cloud products CLAAS Edition 3	Doc. No: SAF/CM/KNMI/PUM/SEV/CLD Issue: 3.1 Date: 08.08.2022
---	--	--

vector contains outer limits of the cloud droplet number concentration (CDNC) bins

hist1d_cdnc_bin_centre(hist_cdnc_bin_centre)

vector contains centre of the CDNC bins

hist1d_cgt_bin_border(hist_cgt_bin_border)

vector contains outer limits of the cloud geometrical thickness (CGT) bins

hist1d_cgt_bin_centre(hist_cgt_bin_centre)

vector contains centre of the CGT bins

hist1d_cwp(lon, lat, hist1d_cwp_bin_centre, hist_phase, time)

number of occurrences of specific CWP ranges at given spatial location. Includes IWP and LWP histogram along the *hist_phase* dimension.

hist1d_cot(lon, lat, hist1d_cot_bin_centre, hist_phase, time)

number of occurrences of specific COT ranges at given spatial location.

hist1d_cre(lon, lat, hist1d_cre_bin_centre, hist_phase, time)

number of occurrences of specific CRE ranges at given spatial location.

hist1d_cdnc(lon, lat, hist1d_cdnc_bin_centre, hist_phase, time)

number of occurrences of specific CDNC ranges at given spatial location.

hist1d_cgt(lon, lat, hist1d_cgt_bin_centre, hist_phase, time)


number of occurrences of specific CGT ranges at given spatial location.

Notes:

- The values averaged in cloud water path histograms are based on 0.6 – 3.9 μm retrieval.
- CDNC and CGT histograms are only available for liquid clouds (*hist_phase* = 0), but for consistency they have a *hist_phase* dimension

7.2.3.8 Mean diurnal cycle

The mean diurnal cycle products are provided as daily mean and monthly mean. The values averaged in CPH and LWP/IWP products are based on 0.6 – 3.9 μm retrieval. The spatial resolution of the diurnal cycles is $0.25^\circ \times 0.25^\circ$.

	Product User Manual SEVIRI cloud products CLAAS Edition 3	Doc. No: SAF/CM/KNMI/PUM/SEV/CLD Issue: 3.1 Date: 08.08.2022
---	--	--

The diurnal cycles of following variables are available:

- cloud fractional cover / mean probabilistic cloud mask
- cloud phase
- cloud top temperature/pressure/height
- liquid/ice water path
- liquid/ice optical thickness
- effective droplet radius and effective ice particle size
- cloud droplet number concentration
- liquid cloud geometrical thickness


7.2.4 Global attributes

Table 7-7 contains the global attributes of averaged CLAAS-3 L3 final product files. Possible values of the attributes are also given as well as explanations.


Table 7-7: Overview of global attributes of NetCDF files of CLAAS-3 products and possible corresponding values.

Name	Description
<i>title</i>	CM SAF CCloud property dAtAset using SEVIRI (CLAAS), edition 3
<i>summary</i>	This file contains SEVIRI-based Thematic Climate Data Records (TCDR) produced by the Satellite Application Facility on Climate Monitoring (CM SAF)
<i>id</i>	DOI:10.5676/EUM_SAF_CM/CLAAS/V003
<i>product_version</i>	3.0
<i>creator_name</i>	DE/DWD
<i>creator_email</i>	contact.cmsaf@dwd.de
<i>creator_url</i>	https://www.cmsaf.eu/
<i>institution</i>	EUMETSAT/CMSAF
<i>project</i>	Satellite Application Facility on Climate Monitoring (CM SAF)

Name	Description
<i>references</i>	https://doi.org/10.5676/EUM_SAF_CM/CLAAS/V003
<i>keywords_vocabulary</i>	Vocabulary for keywords in the global attributes (GCMD Science Keywords, Version 8.6)
<i>keywords</i>	EARTH SCIENCE>ATMOSPHERE>CLOUDS>"variable group"
<i>conventions</i>	convention tables for metadata and attributes (CF-1.7, ACDD-1.3)
<i>standard_name_vocabulary</i>	Vocabulary for standard names in the parameter attributes (Standard Name Table (v70, 10 December 2019))
<i>date_created</i>	Point in time, when the file was created [ISO8601 date]
<i>geospatial_lat_max</i>	90
<i>geospatial_lat_min</i>	-90
<i>geospatial_lat_units</i>	degrees_north
<i>geospatial_lon_max</i>	90
<i>geospatial_lon_min</i>	-90
<i>geospatial_lon_units</i>	degrees_east
<i>geospatial_lat_resolution</i>	0.05 degrees / 0.25 degrees
<i>geospatial_lon_resolution</i>	0.05 degrees / 0.25 degrees
<i>time_coverage_start</i>	Temporal coverage start of the data [ISO8601 date]
<i>time_coverage_end</i>	Temporal coverage end of the data [ISO8601 date]
<i>time_coverage_duration</i>	P1M or P1D (period 1 month or day)
<i>time_coverage_resolution</i>	P1M or P1D or PT1H (period 1 month or day or hour)

	Product User Manual SEVIRI cloud products CLAAS Edition 3	Doc. No: SAF/CM/KNMI/PUM/SEV/CLD Issue: 3.1 Date: 08.08.2022
---	--	--

Name	Description
<i>platform_vocabulary</i>	Vocabulary for platform in the global attributes (GCMD Platforms, Version 8.6)
<i>instrument_vocabulary</i>	Vocabulary for instrument in the global attributes (GCMD Instruments, Version 8.6)
<i>instrument</i>	Earth Remote Sensing Instruments>Passive Remote Sensing >Spectrometers/Radiometers>Imaging Spectrometers/Radiometers>SEVIRI>Spinning Enhanced Visible and Infrared Imager
<i>CMSAF_included_Daily_Means</i>	For monthly means, this attribute counts the number of daily means, that are used to build the monthly mean
<i>CMSAF_repeat_cycles</i>	For daily means, this attribute contains the METEOSAT number and it counts the number of repeat cycles, that are used to build the daily mean
<i>CMSAF_L2_processor</i>	NWC/PPS version v2018 patch5 + CmsafPpsSeviri 0.5.0, CPP v6.0
<i>CMSAF_L3_processor</i>	CMSAFMSG3_V3.0
<i>platform</i>	Earth Observation Satellites > METEOSAT > METEOSAT-8 (or 9 or 10 or 11)
<i>license</i>	<p>The CM SAF data are owned by EUMETSAT and are available to all users free of charge and with no conditions to use. If you wish to use these products, EUMETSAT's copyright credit must be shown by displaying the words "Copyright (c) (2022) EUMETSAT" under/in each of these SAF Products used in a project or shown in a publication or website.</p> <p>Please follow the citation guidelines given at https://doi.org/10.5676/EUM_SAF_CM/CLAAS/V003 and also register as a user at http://cm-saf.eumetsat.int/ to receive latest information on CM SAF services and to get access to the CM SAF User Help Desk.</p>
<i>variable_id</i>	names of the main variables in the product

	Product User Manual SEVIRI cloud products CLAAS Edition 3	Doc. No: SAF/CM/KNMI/PUM/SEV/CLD Issue: 3.1 Date: 08.08.2022
---	--	--

8 Data ordering via the Web User Interface (WUI)

User services are provided through the CM SAF homepage www.cmsaf.eu. The user service includes information and documentation about the CM SAF and the CM SAF products, information on how to contact the user help desk and allows to search the product catalogue and to order products.

On the main webpage, a detailed description how to use the web interface for product search and ordering is given. We refer the user to this description since it is the central and most up to date documentation. However, some of the key features and services are briefly described in the following sections.

8.1 Product ordering process

You need to be registered and logged in to order products. A login is provided upon registration, all products are delivered free of charge. After the selection of the product, the desired way of data transfer can be chosen. This is either via a temporary ftp account (the default setting), or by CD/DVD or email. Each order will be confirmed via email, and the user will get another email once the data have been prepared. If the ftp data transfer was selected, this second email will provide the information on how to access the ftp server.

8.2 Contact User Help Desk staff


In case of questions the contact information of the User Help Desk (e-mail address contact.cmsaf@dwd.de, telephone and fax number) are available via the CM SAF main webpage (<https://www.cmsaf.eu>) or the main page of the Web User Interface.

8.3 Feedback/User Problem Report

Users of CM SAF products and services are encouraged to provide feedback on the CM SAF product and services to the CM SAF team. Users can either contact the User Help Desk (see chapter 8.2) or use the “User Problem Report” page. A link to the “User Problem Report” is available either from the CM SAF main page (www.cmsaf.eu) or the Web User Interface main page.

8.4 Service Messages / log of changes

Service messages and a log of changes are also accessible from the CM SAF main webpage (www.cmsaf.eu) and provide useful information on product status, versioning and known deficiencies.

	Product User Manual SEVIRI cloud products CLAAS Edition 3	Doc. No: SAF/CM/KNMI/PUM/SEV/CLD Issue: 3.1 Date: 08.08.2022
---	--	--

9 Copyright and Disclaimer

The user of CM SAF data agrees to respect the following regulations:

Copyright

All intellectual property rights of the CM SAF products belong to EUMETSAT. The use of these products is granted to every interested user, free of charge. If you wish to use these products in publications, presentations, web pages etc., EUMETSAT's copyright credit must be shown by displaying the words "copyright (year) EUMETSAT" on each of the products used.

Acknowledgement and Identification

When exploiting EUMETSAT/ CM SAF data you are kindly requested to acknowledge this contribution accordingly and make reference to the CM SAF, e.g. by stating "The work performed was done (i.a.) by using data from EUMETSAT's Satellite Application Facility on Climate Monitoring (CM SAF)". It is highly recommended to clearly identify the product version used. An effective way to do this is the citation of CM SAF data records via the digital object identifier (doi). The doi of the data sets can be retrieved through (<http://www.cmsaf.eu/DOI>).

Re-distribution of CM SAF data


Please do not re-distribute CM SAF data to 3rd parties. The use of the CM SAF products is granted free of charge to every interested user, but we have an essential interest to know how many and what users the CM SAF has. This helps to ensure of the CM SAF operational services as well as its evolution according to user needs and requirements. Each new user shall register at CM SAF in order to retrieve the data.

Feedback

We are keen to learn of what use the CM SAF data are. So please feedback your experiences and your application area of the CM SAF data. EUMETSAT CM SAF is user driven service and is committed to consider the needs and requirements of its users in the planning for product improvements and additions. Users are invited to provide their specific requirements on future products for their applications.

10 References

- Alexandri, G., Georgoulas, A.K., Meleti, C., Balis, D., Kourtidis, K.A., Sanchez-Lorenzo, A., Trentmann, J. and Zanis, P., 2017. A high resolution satellite view of surface solar radiation over the climatically sensitive region of Eastern Mediterranean. *Atmospheric Research*, 188, pp.107-121.
- Alexandri, G., Georgoulas, A. K., Zanis, P., Katragkou, E., Tsikerdekis, A., Kourtidis, K., and Meleti, C., 2015: On the ability of RegCM4 regional climate model to simulate surface solar radiation patterns over Europe: an assessment using satellite-based observations, *Atmos. Chem. Phys.*, 15, 13195-13216, doi:10.5194/acp-15-13195-2015.
- Baum, B. A., P. Yang, A. J. Heymsfield, C. G. Schmitt, Y. Xie, A. Bansemer, Y.-X. Hu, and Z. Zhang, 2011: Improvements in shortwave bulk scattering and absorption models for the remote sensing of ice clouds
- Benas, N., Finkensieper, S., Stengel, M., van Zadelhoff, G.-J., Hanschmann, T., Hollmann, R., and Meirink, J. F., 2017: The MSG-SEVIRI-based cloud property data record CLAAS-2, *Earth System Science Data*, 9, 415–434, doi:10.5194/essd-9-415-2017.
- Bennartz, R. and J. Rausch, 2017: Global and regional estimates of warm cloud droplet number concentration based on 13 years of AQUA-MODIS observations, *Atmos. Chem. Phys.*, 17, 9815-9836, doi:10.5194/acp-17-9815-2017.
- Bruno, O., Hoose, C., Storelvmo, T., Coopman, Q., and Stengel, M.: Exploring the cloud top phase partitioning in different cloud types using active and passive satellite sensors, *Geophysical Research Letters*, 48, e2020GL089863-e082020GL089863, <https://doi.org/10.1029/2020GL089863>, 2021.
- Coakley, J. A., M. A. Friedman, and W. R. Tahnk, 2005: Retrieval of cloud properties for partly cloudy imager pixels, *J. Atmos. Ocean. Technol.*, 22 , 3–17.
- Coopman, Q., Hoose, C., and Stengel, M., 2021: Analyzing the thermodynamic phase partitioning of mixed phase clouds over the southern ocean using passive satellite observations, *Geophysical Research Letters*, 48, doi:10.1029/2021GL093225.
- De Haan, J. F., P. Bosma, and J. W. Hovenier, 1987: The adding method for multiple scattering calculations of polarized light, *Astron. Astrophys.*, 183, 371-391.
- Egli, S.; Thies, B.; Bendix, J., 2018: A Hybrid Approach for Fog Retrieval Based on a Combination of Satellite and Ground Truth Data, *Remote Sens.*, 10, 628, doi:10.3390/rs10040628.
- Fuchs, J., Cermak, J., Andersen, H., Hollmann, R. and Schwarz, K., 2017: On the Influence of Air Mass Origin on Low-Cloud Properties in the Southeast Atlantic. *Journal of Geophysical Research: Atmospheres*, 122, 11076-11091, doi:10.1002/2017JD027184.
- Garcia-Carreras, L., J.H. Marsham, and D.V. Spracklen, 2017: Observations of Increased Cloud Cover over Irrigated Agriculture in an Arid Environment. *J. Hydrometeor.*, 18, 2161–2172, <https://doi.org/10.1175/JHM-D-16-0208.1>.

	Product User Manual SEVIRI cloud products CLAAS Edition 3	Doc. No: SAF/CM/KNMI/PUM/SEV/CLD Issue: 3.1 Date: 08.08.2022
---	--	--

Goyens, C., D. Lauwaet, M. Schröder, M. Demuzere, N. van Lipzig, 2011: Tracking Mesoscale Convective Systems in the Sahel: relation between cloud parameters and precipitation, *Int. J. Clim.*, doi: 10.1002/joc.2407.

Greuell, W., E. van Meijgaard, J.F. Meirink, and N. Clerbaux, 2011: Evaluation of model predicted top-of-atmosphere radiation and cloud parameters over Africa with observations from GERB and SEVIRI, *J. Climate*, 25, 4015 – 4036, doi:10.1175/2011JCLI3856.1.

Gristey, J. J., Chiu, J. C., Gurney, R. J., Morcrette, C. J., Hill, P. G., Russell, J. E., and Brindley, H. E., 2018: Insights into the diurnal cycle of global Earth outgoing radiation using a numerical weather prediction model, *Atmos. Chem. Phys.*, 18, 5129-5145, doi:10.5194/acp-18-5129-2018.

Hamann, U., et al., Remote sensing of cloud top pressure/height from SEVIRI: analysis of ten current retrieval algorithms, 2014: *Atmospheric Measurement Techniques*, 7, 2839-2867, doi:10.5194/amt-7-2839-2014.

Haywood, J.M., S.R. Osborne, S.J. Abel, 2004: The effect of overlying absorbing aerosol layers on remote sensing retrievals of cloud effective radius and cloud optical depth, *Quart. J. Roy. Meteorol. Soc.*, 130, 779-800, doi: 10.1256/qj.03.100.

Heidinger, A. K., M. J Foster, A. Walther and X. Zhao, 2013: The Pathfinder Atmospheres Extended (PATMOS-x) AVHRR Climate Data Set., *Bull. Amer. Meteor. Soc*, doi: <http://dx.doi.org/10.1175/BAMS-D-12-00246.1>.

Hill, P. G., R. P. Allan, J. C. Chiu, and T. H. M. Stein, 2016: A multisatellite climatology of clouds, radiation, and precipitation in southern West Africa and comparison to climate models, *J. Geophys. Res. Atmos.*, 121, 10,857–10,879, doi:10.1002/2016JD025246.


Håkansson, N., Adok, C., Thoss, A., Scheirer, R., and Hörnquist, S.: Neural network cloud top pressure and height for MODIS, *Atmos. Meas. Tech.*, 11, 3177–3196, <https://doi.org/10.5194/amt-11-3177-2018>, 2018.

Karlsson, K.-G.; Johansson, E.; Håkansson, N.; Sedlar, J.; Eliasson, S. Probabilistic Cloud Masking for the Generation of CM SAF Cloud Climate Data Records from AVHRR and SEVIRI Sensors. *Remote Sens.* 2020, 12, 713. <https://doi.org/10.3390/rs12040713>

Kuell, V. and A. Bott, 2009: Application of the hybrid convection parameterization scheme HYMACS to different meteorological situations, *Atmos. Res.*, 94, 743-753, doi:10.1016/j.atmosres.2009.04.002.

MacQueen, J. B., 1967: Some Methods for classification and Analysis of Multivariate Observations. *Proceedings of 5th Berkeley Symposium on Mathematical Statistics and Probability*. Vol. 1. University of California Press. pp. 281–297. MR 0214227.

Maddux, B. C., Ackerman, S. A., Platnick, S, 2010: Viewing Geometry Dependencies in MODIS Cloud Products, *J. Atm. Ocean. Tech.*, 27(9), 1519-1528.

	Product User Manual SEVIRI cloud products CLAAS Edition 3	Doc. No: SAF/CM/KNMI/PUM/SEV/CLD Issue: 3.1 Date: 08.08.2022
---	--	--

Marshak, A., S. Platnick, T. Várnai, G. Wen, and R. F. Cahalan, 2006: Impact of three-dimensional radiative effects on satellite retrievals of cloud droplet sizes, *J. Geophys. Res.*, 111, 9207–9218.

Meirink, J.F., R.A. Roebeling and P. Stammes, 2013: Inter-calibration of polar imager solar channels using SEVIRI, *Atm. Meas. Tech.*, 6, 2495-2508, doi:10.5194/amt-6-2495-2013.

Nakajima, T., and M. D. King, 1990: Determination of the Optical Thickness and Effective Particle Radius of Clouds from Reflected Solar Radiation Measurements. Part 1: Theory. *J. Atmos. Sci.*, 47, 1878-1893.

Nickovic, S., Cvetkovic, B., Madonna, F., Rosoldi, M., Pejanovic, G., Petkovic, S., and Nikolic, J.: Cloud ice caused by atmospheric mineral dust – Part 1: Parameterization of ice nuclei concentration in the NMME-DREAM model, *Atmos. Chem. Phys.*, 16, 11367-11378, doi:10.5194/acp-16-11367-2016, 2016.

Pan, Z., Rosenfeld, D., Zhu, Y., Mao, F., Gong, W., Zang, L., and Lu, X., 2021: Observational quantification of aerosol invigoration for deep convective cloud lifecycle properties based on geostationary satellite. *Journal of Geophysical Research: Atmospheres*, 126, doi:10.1029/2020JD034275.

Pfeifroth, U., R. Hollmann, and B. Ahrens, 2012: Cloud cover diurnal cycles in satellite data and regional climate model simulations, *Meteorologische Zeitschrift*, 21, 551-560.

Platnick, S., 2001: A superposition technique for deriving mean photon scattering statistics in plane-parallel cloudy atmospheres, *J. Quant. Spectrosc. Radiat. Transfer*, 68, 57-73.


Roebeling, R. A., A. J. Feijt, and P. Stammes, 2006: Cloud property retrievals for climate monitoring: implications of differences between SEVIRI on METEOSAT-8 and AVHRR on NOAA-17, *J. Geophys. Res.*, 111, D20210, doi:10.1029/2005JD006990.

Roebeling, R. A., and E. van Meijgaard, 2009: Evaluation of the Daylight Cycle of Model-Predicted Cloud Amount and Condensed Water Path over Europe with Observations from MSG SEVIRI, *J. Clim.*, 22 (7), 1749-1766 DOI: 10.1175/2008JCLI2391.1.

Ruiz-Arias, J.A., C. Arbizu-Barrena, F.J. Santos-Alamillos, J. Tovar-Pescador, and D. Pozo-Vázquez, 2016: Assessing the Surface Solar Radiation Budget in the WRF Model: A Spatiotemporal Analysis of the Bias and Its Causes. *Mon. Wea. Rev.*, 144, 703–711, doi:10.1175/MWR-D-15-0262.1.

Rybka, H., Burkhardt, U., Köhler, M., Arka, I., Bugliaro, L., Görsdorf, U., Horváth, Á., Meyer, C. I., Reichardt, J., Seifert, A., and Strandgren, J., 2021: The behavior of high-CAPE (convective available potential energy) summer convection in large-domain large-eddy simulations with ICON, *Atmos. Chem. Phys.*, 21, 4285–4318, <https://doi.org/10.5194/acp-21-4285-2021>.

Seethala, C., Meirink, J. F., Horvath, A., Bennartz, R., and Roebeling, R., 2018: Evaluating the diurnal cycle of South Atlantic stratocumulus clouds as observed by MSG SEVIRI, *Atmospheric Chemistry and Physics*, 18, 13 283–13 304, doi:10.5194/acp-18-13283-2018.

	Product User Manual SEVIRI cloud products CLAAS Edition 3	Doc. No: SAF/CM/KNMI/PUM/SEV/CLD Issue: 3.1 Date: 08.08.2022
---	--	--

Stammes, P., 2001: Spectral radiance modeling in the UV-Visible range. IRS 2000: Current problems in Atmospheric Radiation, edited by W.L. Smith and Y.M. Timofeyev, pp 385-388, A. Deepak Publ., Hampton, VA.

Stengel, M., Kniffka, A., Meirink, J. F., Lockhoff, M., Tan, J., and Hollmann, R., 2014: CLAAS: the CM SAF cloud property data set using SEVIRI, *Atmos. Chem. Phys.*, 14, 4297–4311.

Taylor, S., Stier, P., White, B., Finkensieper, S., and Stengel, M., 2017: Evaluating the diurnal cycle in cloud top temperature from SEVIRI, *Atmos. Chem. Phys.*, 17, 7035-7053, doi:10.5194/acp-17-7035-2017.

Teuling, A. J., Taylor, C. M., Meirink, J. F., Melsen, L. A., Miralles, D. G., van Heerwaarden, C. C., Vautard, R., Stegehuis, A. I., Nabuurs, G.-J., and de Arellano, J. V.-G.: Observational evidence for cloud cover enhancement over western European forests, *Nature Communications*, 8, 14 065, doi:10.1038/ncomms14065, 2017.

Van Weverberg K., van Lipzig N.P.M., Delobbe L., Vogelmann A.M., 2012: The role of precipitation size distributions in km-scale NWP simulations of intense precipitation: evaluation of cloud properties and surface precipitation. *Q. J. R. Meteorol. Soc.* DOI:10.1002/qj.1933.

Yang, P., L. Bi, B. A. Baum, K.-N. Liou, G. W. Kattawar, M. I. Mishchenko, and B. Cole, 2013: Spectrally consistent scattering, absorption, and polarization properties of atmospheric ice crystals at wavelengths from 0.2 to 100 μ m, *J. Atmos. Sci.*, 70, 330-347, doi:10.1175/JAS-D-12-039.1.

11 Acronyms

AMSR	Advanced Microwave Scanning Radiometer
ATBD	Algorithm Theoretical Baseline Document
AVHRR	Advanced Very High Resolution Radiometer
BC-RMS	Bias-Corrected RMS
CALIOP	Cloud-Aerosol Lidar with Orthogonal Polarisation
CALIPSO	Cloud-Aerosol Lidar and Infrared Pathfinder Satellite Observations
CDO	Climate Data Operators
CDOP	Continuous Development and Operations Phase
CFC	Fractional Cloud Cover
ICOT	Integrated Cloud Optical Thickness
CLARA-A	CM SAF cLoud, Albedo and Radiation products, AVHRR-based
CLAAS	CM SAF cLoud dAtAset using SEVIRI
CM SAF	Satellite Application Facility on Climate Monitoring
COT	Cloud Optical Thickness
CPH	Cloud Phase
CPR	Cloud Profiling Radar
CRE	Cloud particle effective radius
CTH	Cloud Top Height
CTO	Cloud Top product
CTP	Cloud Top Pressure
CTT	Cloud Top Temperature
CPP	Cloud Physical Properties
DAK	Doubling Adding KNMI (radiative transfer model)
DARDAR	raDAR/iIDAR
DOI	Digital Object Identifier
DRR	Delivery Readiness Review
DWD	Deutscher Wetterdienst (German Met Service)
ECMWF	European Centre for Medium Range Forecast
ECV	Essential Climate Variable
ERA5	ECMWF Re-Analysis 5
EUMETSAT	European Organisation for the Exploitation of Meteorological Satellites
EWC	EUMETSAT Weather Cloud

FAR	False Alarm Ratio
FCDR	Fundamental Climate Data Record
FCI	Flexible Combined Imager
GCOS	Global Climate Observing System
GSICS	Global Space-Based Inter-Calibration System
ICDR	Interim Climate Data Record
IR	InfraRed
ISCCP	International Satellite Cloud Climatology Project
ITCZ	Inter Tropical Convergence Zone
IWP	Ice Water Path
JCH	Joint Cloud properties Histogram
KNMI	Koninklijk Nederlands Meteorologisch Instituut (Dutch Met Service)
KSS	Hanssen-Kuipers Skill Score
L1.5	Level 1.5
L2	Level 2
L3	Level 3
LWP	Liquid Water Path
MAC-LWP	Multisensor Advanced Climatology of Liquid Water Path (data record)
MODIS	Moderate Resolution Imaging Spectroradiometer
MSG	Meteosat Second Generation
MTG	Meteosat Third Generation
NIR	Near InfraRed
NOAA	National Oceanic & Atmospheric Administration
NWC SAF	SAF in support of Nowcasting and Very Short Range Forecasting
NWP	Numerical Weather Prediction
PATMOS-x	Pathfinder Atmospheres-Extended dataset (NOAA)
POD	Probability Of Detection
PPS	Polar Platform System (NWC SAF polar cloud software package)
PRD	Product Requirement Document
PUM	Product User Manual
RMSE/RMSD	Root Mean Square Error/Difference
RTM	Radiative Transfer Model
RTTOV	Radiative Transfer model for TOVS

SEVIRI	Spinning Enhanced Visible and InfraRed Imager
SAF	Satellite Application Facility
SMHI	Swedish Meteorological and Hydrological Institute
SYNOP	Synoptic observations
SZA	Solar Zenith Angle
TCDR	Thematic Climate Data Record
VIS	Visible
VZA	Viewing Zenith Angle